

Introduction to machine learning potentials for atomistic simulations

Fabian L. Thiemann,^{1,2} Niamh O’Neill,^{3,2,4} Venkat Kapil,^{3,4,5,6} Angelos Michaelides,^{3,4} and Christoph Schran^{2,4, a)}

¹⁾ IBM Research Europe, Daresbury, Warrington, WA4 4AD, UK

²⁾ Cavendish Laboratory, Department of Physics, University of Cambridge, Cambridge, CB3 0HE, UK

³⁾ Yusuf Hamied Department of Chemistry, University of Cambridge, Lensfield Road, Cambridge, CB2 1EW, UK

⁴⁾ Lennard-Jones Centre, University of Cambridge, Trinity Ln, Cambridge, CB2 1TN, UK

⁵⁾ Department of Physics and Astronomy, University College London, London, UK

⁶⁾ Thomas Young Centre and London Centre for Nanotechnology, London, UK, London, UK

(Dated: 2 October 2024)

Machine learning potentials have revolutionised the field of atomistic simulations in recent years and are becoming a mainstay in the toolbox of computational scientists. This paper aims to provide an overview and introduction into machine learning potentials and their practical application to scientific problems. We provide a systematic guide for developing machine learning potentials, reviewing chemical descriptors, regression models, data generation and validation approaches. We begin with an emphasis on the earlier generation of models, such as high-dimensional neural network potentials (HD-NNPs) and Gaussian approximation potential (GAP), to provide historical perspective and guide the reader towards the understanding of recent developments, which are discussed in detail thereafter. Furthermore, we refer to relevant expert reviews, open-source software, and practical examples – further lowering the barrier to exploring these methods. The paper ends with selected showcase examples, highlighting the capabilities of machine learning potentials and how they can be applied to push the boundaries in atomistic simulations.

I. Introduction	2	C. Beyond Locality	18
II. Chemical Descriptors	3	D. General Purpose and Foundational Models	19
A. Atom-Centred Symmetry Functions	3	V. Data Set Generation	19
B. Smooth Overlap of Atomic Positions	5	A. Structural Selection Techniques	20
C. Discussion and Outlook on Chemical Descriptors	6	B. Active Learning	20
III. Regression Models	8	C. Reinforcement Workflows	21
A. Artificial neural networks	8	VI. Validation	21
1. High-dimensional Neural Network Potentials	9	A. Primary Properties and Numerical Errors	22
2. Obtaining Analytical Derivatives	10	B. Validation of Secondary Properties	23
3. Training	10	VII. Showcase Examples	24
B. Gaussian Process and Kernel Ridge Regression	11	VIII. Summary and Outlook	26
1. Weight-Space View	11	Acknowledgments	28
2. Function-Space View	13	Competing interests	28
3. Gaussian Approximation Potentials	14	Supporting Information	28
C. Discussion and Outlook of Regression Models	16	Overview of Machine Learning Concepts	S1
IV. Current Developments	17	Overview of Open-Source Code	S2
A. Completeness of Descriptors	17		
B. Learnable Descriptors: Graph Neural Networks	18		

^{a)} Electronic mail: cs2121@cam.ac.uk

I. INTRODUCTION

Most of the chemistry and physics of molecular systems and materials is governed by the potential energy surface (PES). Within the Born-Oppenheimer approximation, the properties of a system of interest can thus be obtained from its thermally weighted population on the ground state PES, as sampled either by molecular dynamics or Monte Carlo techniques. Having access to an accurate but efficient representation of the system’s PES is therefore of paramount importance for the computational study of material properties, reactions, and molecular processes. While *ab initio* techniques such as density functional theory (DFT) can provide the required accuracy for a large variety of complex systems, they are usually relatively expensive as the electronic structure of each sampled configuration needs to be obtained. This cost comes from the challenges associated with approximating the many-body Schrödinger equation, in particular, due to the electron-electron repulsion. Force field techniques, on the other hand, use a set of usually physically motivated functions for different types of interaction to represent the PES with parameters optimized to either match experiments or higher-level electronic structure data. These are usually quite efficient but in many cases not accurate enough or are missing reactivity in order to provide reliable insight.

In recent times, the use of machine learning has enabled the PES to be learned from the previously solved electronic structure of a set of configurations in order to provide reliable interpolation at a cost similar to FF methods, but reproducing the accuracy of *ab initio* techniques.^{1–12} The generality and data-driven nature of these approaches has led to a surge in the use and development of machine-learning techniques for atomistic simulations. The field of machine learning potentials (MLPs) has grown quickly in the last couple of years after the seminal works of Behler and Parrinello in 2007¹³ using artificial neural networks and Bartók and coworkers using Kernel-based approaches in 2010.¹⁴ Nowadays, there is a wide variety of methods and just some examples include moment-tensor potentials,^{15,16} atomic cluster expansion,¹⁷ spectral neighbour analysis potentials,^{18,19} message-passing based neural networks^{20–24} and deep learning methods.^{25–27} Typically, MLPs are made up of two main components: an encoding strategy that represents the molecular structure (commonly referred to as descriptors) and a regression technique mapping the atomic configuration space to the PES. These models can be trained on data generated by electronic structure calculations and then used to make predictions for systems that are too large or complex to be treated with such methods. Another advantage of these machine learning approaches is that they can be easily parallelized, which allows for efficient calculations on high-performance computing platforms.^{28–31} Overall, the use of machine learning in atomistic simulations is a vibrant

area of research that is greatly enhancing the accuracy and efficiency of molecular and materials modelling.

The aim of this tutorial is to bridge the gap between the theoretical formalism of machine-learning methods and their application by providing a practical guide for those interested in implementing machine-learning-based methods in their research. It is particularly targeted at those with some experience in molecular simulations but who want to understand more about the practicalities of training and applying MLPs to their system of interest. To enable a broader understanding but also facilitate comparisons, in each section, we will first describe the general principles applicable to all approaches and then focus on specific methods, which can then be contrasted. In particular, the two most common flavours of MLPs, artificial neural networks and Gaussian process regression and their associated descriptors, will be a particular focus – given their well-established software and literature available, they are very accessible to the ML beginner. We start with the two first established variants in both of these categories, the so-called high-dimensional neural network potentials (HD-NNPs)¹³ and Gaussian approximation potentials (GAPs),¹⁴ as a gateway for more recent approaches discussed afterwards. The motivation for this is that core ideas remain mostly constant, and new developments thus can be best understood in their historical context. For the tutorial to be of direct practical use, we also compile in Tab. S2 of the supporting information, some of the open-source software available for various tasks and provide a Colab tutorial that exemplifies all the steps of the development process of an MLP.

The field has experienced a significant surge in recent years, leading to an abundance of expert reviews on diverse aspects of MLPs authored by renowned pioneers. This includes multiple excellent reviews on the HD-NNP^{32–35} and GAP^{36,37} formalism, as well as other broader reviews.^{5,11,38–40} In addition, special areas have been covered, such as structural representation by chemical descriptors,⁴¹ learning of excited states,⁴² machine learning in chemical compound space,⁴³ focus on small molecules⁴⁴ and reactions,⁴⁵ inclusion of long-range effects,⁴⁶ as well as dataset generation techniques.⁴⁷ Complementing this work, our aim is to present an entry-level description of the methodology, encompassing a broad part of this rapidly expanding field. We hope this can serve as a solid foundation for further exploration using the aforementioned resources. While the GAP and HD-NNP formalisms and later developments have all been reviewed in detail before, they have not been directly contrasted in a tutorial-style paper as an introduction for beginners. Thus, this tutorial will function as a gateway to the more detailed and advanced material to facilitate further uptake of the methods in the everyday toolbox of computational scientists.

The basic idea behind machine learning in the current context is to assemble a set of reference points for which the property is going to be “learned” is known. This

is usually done in an automated procedure in order to prevent as much user input as possible. In the field of supervised learning, the properties (also called labels) of the reference points need to be curated by the user before being learned by the machine learning algorithm. This preparation of the input is, in many cases, very important for the quality of the outcome, since a clear differentiation between individual points in the reference set needs to be achieved. Once a meaningful data set has been prepared, a universal functional form with large parameter sets is optimised to match the reference values (referred to as regression). Afterwards, the model can be applied for fast and highly accurate interpolation between the points in the reference set.

Within this beginner’s guide, we will see how the concepts of machine learning can be applied in atomistic simulations in order to “learn” efficient and reactive forms of the PES. The main concepts shared by most approaches are summarised in Figure 1. In order to construct a representative structure-energy relation, the structure is usually first transformed by a set of descriptors to provide more meaningful input for the actual machine-learning model. In most cases, these descriptors are atom-centred and limited to a certain spherical cutoff, thus yielding a fingerprint of the chemical environment around each atom. This means that locality is usually built into such models, enabling linear scaling with the number of atoms. The machine learning model is then trained to reproduce energies (and forces as the first derivative of the PES) for a curated set of labeled configurations. This is done by optimizing the parameters of the model in order to minimize the difference between the model’s prediction and the reference values. Afterwards, the model is able to provide reliable predictions for unseen configurations as long as sufficiently similar configurations have been present in the training data. We refer the novice reader to Tab. S1 for a short overview of the central concepts of machine learning relevant for this tutorial.

In the next sections, we will go over the details of these various steps in developing MLPs. First, chemical descriptors will be introduced where the main focus will be on radial and angular descriptors as well as atomic density. Next, two of the most well-established and common machine learning approaches, artificial neural networks and Gaussian process regression models will be presented, as well as how they can be combined with descriptors to provide robust and accurate structure-energy mappings. We will then shift to strategies for the generation of representative data sets, as well as validation techniques. Finally, we end with an overview of showcase examples as well as an outlook on new developments in the field and techniques, such as going beyond ground-state PES and representing other properties.

II. CHEMICAL DESCRIPTORS

PESs have some intrinsic properties when it comes to their dependence on structure: Imagine translating, rotating, or reflecting a molecule. All three operations do not influence the potential energy of the system, as long as no external potential is applied. This means that the potential energy is invariant with respect to these three operations. Similarly, the order of the atoms should not influence the energy either, resulting in an invariance with respect to permutations. Therefore, when constructing a mathematical relationship between structure and energy, it is crucial to think about how the structural information is encoded as input for the machine learning model.^{41,48,49} It is possible to construct a PES without considering these inherent invariances, but it means that the data set needs to provide sufficient information on differently rotated, translated, and permuted systems, or the model itself must be able to recover the invariances from the input. In such cases, Cartesian coordinates or similar measures like distance matrices, collecting all $N \times N$ distances between all atoms in the system, as well as their inverse (called Coulomb matrices),⁵⁰ are used to describe the chemical structure. Early work captured the rotational and translational invariances using internal coordinate systems.^{51–53} However, this still did not solve the issue of permutational invariance. Usually, it is easier to incorporate the invariances by transforming the Cartesian coordinates into a more representative form that intrinsically accounts for the required invariances.

In the following, we will see how two different types of descriptors can be used to represent chemical environments and how the required invariances are included. First, so-called atom-centred symmetry functions are introduced, which probe the radial and angular environment within a certain cutoff. The second example of descriptors is the so-called smooth overlap of atomic positions, relying on a density representation of the atoms that are expanded as many-body expressions. Finally, we will give a brief overview of the limitations of these widely used descriptors and provide examples of more modern variants.

A. Atom-Centred Symmetry Functions

Atom-centred symmetry functions (ACSFs)^{13,54,55} and variants^{56,57} have been introduced as a way to encode the chemical fingerprint around each atom in a system while incorporating the translational, rotational and permutational invariance. They rely on a set of radial and angular functions that probe different regions in the vicinity of each atom up to a predefined cutoff. For both the ra-

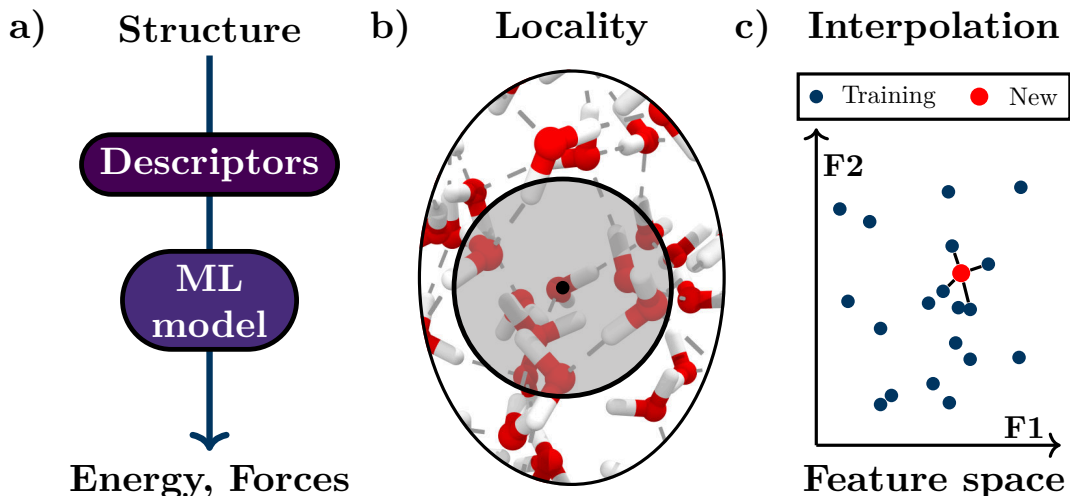


FIG. 1. **Overview of the main principles of machine learning potentials.** a) Structure is related to energy and forces in a two-step process using chemical descriptors as input for the machine learning regression model. b) Most descriptors in the field are limited to a certain cutoff around each atom, building a locality approximation into the formalism as illustrated here by the grey-shaded region centred on the central oxygen atom. c) The main task of the machine learning potential is then, after training, to interpolate between the known and representative training data for previously unseen configurations. This is illustrated here within a simple two-dimensional feature space.

dial and angular symmetry functions, a cutoff function, such as

$$f_c(R_{ij}) = \begin{cases} 0.5 \cdot \left[\cos\left(\frac{\pi R_{ij}}{R_c}\right) + 1 \right] & \text{for } R_{ij} \leq R_c \\ 0 & \text{else} \end{cases} \quad (1)$$

is used. Here, R_{ij} is the distance between the central atom i and a neighbouring atom j , used to define the atomic environment up to a certain cutoff radius R_c . The radial arrangement of the atoms within this cutoff sphere is accounted for by a product of a Gaussian and the cutoff function according to Eq. (1),

$$G_i^{\text{rad}} = \sum_j e^{-\eta(R_{ij}-R_s)^2} \cdot f_c(R_{ij}) \quad , \quad (2)$$

where different regions around the central atom i can be probed by adapting the width of the Gaussian η and the shifting parameter R_s . To complement the description of the environment around each atom, angular functions of the form

$$G_i^{\text{ang}} = 2^{1-\zeta} \sum_{j,k \neq i, j \neq k} (1 + \lambda \cos \theta_{ijk})^\zeta \cdot e^{-\eta(R_{ij}^2 + R_{ik}^2 + R_{jk}^2)} \cdot f_c(R_{ij}) \cdot f_c(R_{ik}) \cdot f_c(R_{jk}) \quad (3)$$

are employed. These depend on the angle θ_{ijk} between the central atom i and two neighbours j and k , where i, j and k can be any atom of the system of interest. Different angular regions are probed by adjusting the exponent ζ . The parameter λ , which can have values of $+1$ or -1 , is used to shift the maximum of the cosine either to π or 2π .

The different parameters ($R_c, \eta, R_s, \zeta, \lambda$) are so-called hyperparameters of the model and need to be chosen by the user. They can vary depending on the system of interest as different chemical systems require different fingerprints for their chemical surrounding. However, in practice, a well-chosen general set of functions can be applied for various systems as long as all relevant regions around the atoms are well represented.

The influence of the different hyperparameters on the shape of the different symmetry functions is shown in Figure 2. The cutoff function smoothly decays to zero when reaching the chosen cutoff value R_c . The radial functions are Gaussian functions of variable width and centred at a chosen position, thus allowing different radial regions around the central atom to be probed. The functional form of the angular ACSFs is a bit more complex due to their angular and radial contribution, but the shape of the angular contribution is sufficient to understand most of its effects: By choosing ζ , the angular component can be made narrower or wider, while λ allows the centre of the angular width to be moved to a different angular value. With these parameters, different angular regions around each atom can be distinguished.

Both radial and angular symmetry functions are evaluated over all distances with atoms of a chosen element up to the cutoff and the resulting value is summed up to give the fingerprint of this element. This means that for each pair and triple of elements, a different set of symmetry functions needs to be specified in order to distinguish all possible chemical environments. A set of functions is required in this case to provide sufficient sensitivity for different radial and angular regions.

For a simple example of a water molecule, one would require two sets of symmetry functions, one for the oxygen atom and one for the hydrogen atoms. The set of ACSFs for the oxygen atom then probes different radial distances with respect to the surrounding hydrogen atoms. This could be achieved, for example, by defining ten radial functions of various widths and shifted to different distances R_s , where the exact number depends on the system of interest and width and shift. If very narrow Gaussians are used, we would need a large set of radial functions to cover the entire cutoff region, while wider ones — although less sensitive — would cover the cutoff region with fewer functions. Furthermore, the angular environment of the oxygen atom could be probed with, e.g. four angular ACSFs that include both hydrogen distances from the central oxygen atom. Again, the number of angular functions is up to the user and depends on the desired sensitivity to different angular regions around the atoms. Other distances (OO) or angles (OHO, OOO) can be omitted as they are not present for a single water molecule. A minimal set of ACSFs for the hydrogen atoms would require some radial functions for the HH and OH distances each, as well as angular functions for the HHO triple. Again, other angular functions for HOO and HHH can be ignored because of the limited number of atoms of the water molecule.

B. Smooth Overlap of Atomic Positions

Developed by Bartók *et al.*,^{14,58} the smooth overlap of atomic positions (SOAP) provides an alternative approach to atom-centred symmetry functions. Aside from being a robust and invariant fingerprint of the atomic environment, SOAP allows for the easy evaluation of the similarity between two environments, making this descriptor particularly powerful for kernel-based regression techniques introduced later. To create the SOAP representation of the environment surrounding a particular atom i , we follow the steps outlined in the bottom of figure 2. First, we construct a set of neighbour densities, $\rho^{i,s}(\mathbf{R})$, one for each atomic species s present in the system. These densities are defined as sums of Gaussians with variance σ_a^2 centred on all atoms of type s within the neighbourhood of atom i :

$$\rho^{i,s}(\mathbf{R}) = \sum_j \delta_{ss_j} e^{-\frac{|\mathbf{R}-\mathbf{R}_{ij}|^2}{2\sigma_a^2}} f_c(R_{ij}), \quad (4)$$

where the index j runs over all neighbours of atom i , including itself, within some cutoff distance R_c . \mathbf{R}_{ij} is the vector pointing from atom i to the neighbour j , and $f_c(R_{ij})$ is a cutoff function that ensures a smooth decay when approaching R_c (as defined in Equation 1). The Kronecker delta δ_{ss_j} ensures that only species of one desired type are considered in each case. The only hyperparameter at this stage aside from the cutoff distance, R_c , is σ_a , which is often associated with the size of the

atoms⁵⁹ and determines the smoothness of the density. Typically, σ_a is set to around 0.3Å when there are hydrogen atoms present in the system to account for the smaller X-H distances and 0.5Å when they are not.³⁷

It is essential to understand that the complete set of elemental neighbour densities are created for each atom i , regardless of the atomic number of atom i . In a water molecule, for example, neighbour densities are always constructed for both hydrogen and oxygen for each central atom, thus resulting in a H and O neighbour density for both hydrogen atoms as well as the oxygen atom. By construction, these individual neighbour densities are invariant to permutations within their respective element type. To eventually ensure rotational invariance, they are expanded in a basis of orthogonal radial functions $G_n(R)$ and spherical harmonics $Y_{lm}(\hat{\mathbf{R}})$ such as

$$\rho^{i,s}(\mathbf{R}) \approx \sum_{\substack{n < n_{\max} \\ l < l_{\max} \\ |m| \leq l}} c_{nlm}^{i,s} G_n(R) Y_{lm}(\hat{\mathbf{R}}), \quad (5)$$

with n , l , and m being integers while l and m are known from quantum mechanics. The choice of the radial basis is not really relevant to the outcome of the procedure as long as it is sufficiently flexible. Indeed, different bases have been used in the literature from orthogonal polynomials to Gaussians. In the given context, n and l are the indices for the radial and angular channels, respectively, and $\hat{\mathbf{R}}$ is the point on the unit sphere corresponding to the direction of the vector \mathbf{R} . In practice, the expansion is truncated at certain values for the radial and angular expansion, represented by the hyperparameters n_{\max} and l_{\max} , respectively. The related expansion coefficients $c_{nlm}^{i,s}$ are given by

$$c_{nlm}^{i,s} = \int d\mathbf{R} G_n(R) Y_{lm}(\hat{\mathbf{R}})^* \rho^{i,s}(\mathbf{R}) \quad (6)$$

from the inverse of equation 5.

Finally, the SOAP descriptor, also known as the SOAP vector, is constructed using the so-called power spectrum of these coefficients

$$p_{nn'l}^{i,ss'} = \frac{1}{\sqrt{2l+1}} \sum_m (c_{nlm}^{i,s})^* c_{n'lm}^{i,s'}, \quad (7)$$

where the sum over m in the context of spherical harmonics corresponds to averaging over all possible rotations, resulting in a rotationally invariant representation. This equation has a lot of indices and it is worthwhile to summarize them again:

- i represents the central atom of choice for which we are obtaining the chemical fingerprint.
- s and s' represent different elements, thus providing information about different combinations of elements in the surroundings.
- Finally, n and n' represent different radial regions of these two element types.

Given this summation over different radial channels, $p_{nn'l}^{i,ss'}$ encodes information about pairs of vectors from the central atom and is therefore of three-body nature. The full SOAP descriptor characterising the environment around a given atom i , $\mathbf{p}^i \equiv \{p_{nn'l}^{i,ss'}\}$, comprises all entries of $p_{nn'l}^{i,ss'}$ resulting in several hundreds or even thousands of components. The length of this vector N^{SOAP} scales quadratically with both the number of elements present in the system N_{ele} and the radial expansion limit, n_{max} , and linearly with the angular expansion limit, l_{max}

$$N^{\text{SOAP}} = \frac{n_{\text{max}}^2 N_{\text{ele}}^2 + n_{\text{max}} N_{\text{ele}}}{2} (l_{\text{max}} + 1). \quad (8)$$

To get a grasp of the dimensions of the SOAP vector, let us consider the descriptors used in previous work. For instance, the SOAP descriptor is constructed to accurately describe pristine graphene⁶⁰ used $n_{\text{max}} = 8$ and $l_{\text{max}} = 8$ resulting in a length of 324 elements. Employing identical expansion limits n_{max} and l_{max} , this value increases to 1,224 for hexagonal boron nitride being composed of two elements B and N.⁶¹ Given the increasing computational cost of calculating SOAP descriptors for complex systems, it is important to carefully choose the hyperparameters n_{max} and l_{max} ^{62,63} and several strategies offer ways to construct a compressed version of the SOAP vector.^{64,65}

While equation 7 provides an invariant and robust representation of the atomic structure, the real power of the SOAP descriptor lies in the convenience of constructing a kernel function which can be used to measure the similarity between two local environments. This makes SOAP a popular choice for kernel-based regression techniques such as Gaussian process regression. The so-called SOAP kernel is calculated by taking the dot product of the normalised power spectrum vectors, $\hat{\mathbf{p}}^i = \mathbf{p}^i / \sqrt{\mathbf{p}^i \cdot \mathbf{p}^i}$, of the local environments. For two environments, A and A' , centred around atoms i and i' , respectively, the SOAP kernel is defined as

$$k(A, A') = \left(\hat{\xi}^i \cdot \hat{\xi}^{i'} \right)^\zeta, \quad (9)$$

where $k(A, A')$ takes values between 0 and 1 corresponding to full dissimilarity or equality of the environments A and A' , respectively. The exponent ζ is an integer that defines the sharpness of the kernel and needs to be > 1 to produce a model beyond three-body terms (see e.g. Ref 37 for a derivation). In fact, many interatomic potentials leveraging the GAP methodology have been developed based on SOAP descriptors employing values of $\zeta = 2$ or $\zeta = 4$.

Finally, let us summarise this whole procedure of obtaining the SOAP descriptor which are also outlined in the bottom of figure 2:

1. Obtain element-specific neighbour densities for each atom in the system.
2. Expand these densities in a radial and angular basis and obtain the resulting expansion coefficients.

3. Build the so-called power spectrum, by combining the expansion coefficient of different elements and radial channels while averaging over the angular components.
4. Normalise the resulting SOAP vector to enable direct comparison between different atomic environments.

While being conceptually a bit more involved than ACSFs, they have the advantage that they are more systematic in the sense that they rely only on two hyperparameters n_{max} and l_{max} (assuming we have a physically motivated guess for σ_a) controlling the radial and angular expansion.

C. Discussion and Outlook on Chemical Descriptors

We have seen that the introduction of a set of general body-ordered functions to transform Cartesian coordinates into an atomic fingerprint enables the required invariances for the representation of PESs with data-driven approaches to be included. From a first glimpse, this might seem quite elaborate as we are transforming $3N_{\text{atom}}$ coordinates into $N_{\text{atom}} \cdot N_{\text{des}}$ descriptors, where the length of the descriptor can easily surpass the thousands. This means that we are arriving at an overcomplete description of our system. However, this additional sensitivity is actually quite useful as it means our regression task can become much easier than for the minimal number of $3N_{\text{atom}} - 6$ internal degrees of freedom. Moreover, it allows the application of the MLP to systems of – in principle – arbitrary size rather than being constrained to the exact number of atoms encountered in systems of the training set.

It is important to note that the transformation via descriptors is not for free. In many cases, it is actually the most costly part of the evaluation of an MLP. In general, as higher body terms are included in the descriptors, the more expensive the computation of the descriptors becomes, due to the steeply rising combinatorial complexity. However, there are certain tricks that can dramatically reduce the cost, which we will come back to in Sec IV.

While being very successful and widely used in many applications, the two presented descriptors have some limitations. One shortcoming of both ACSFs and SOAP vectors is the unfavourable scaling with the number of species in the system. This means that systems on the order of 5-6 different chemical species are currently the limit of what has been described with these descriptors. One way to solve this problem is to account for the element-specific composition of the chemical environment in an implicit manner by introducing element-dependent weighting functions in the descriptors, instead of using separate functions to describe different combinations of elements, as done in weighted ACSFs.⁵⁶ In addition, there are new ideas to sparsify the descriptors

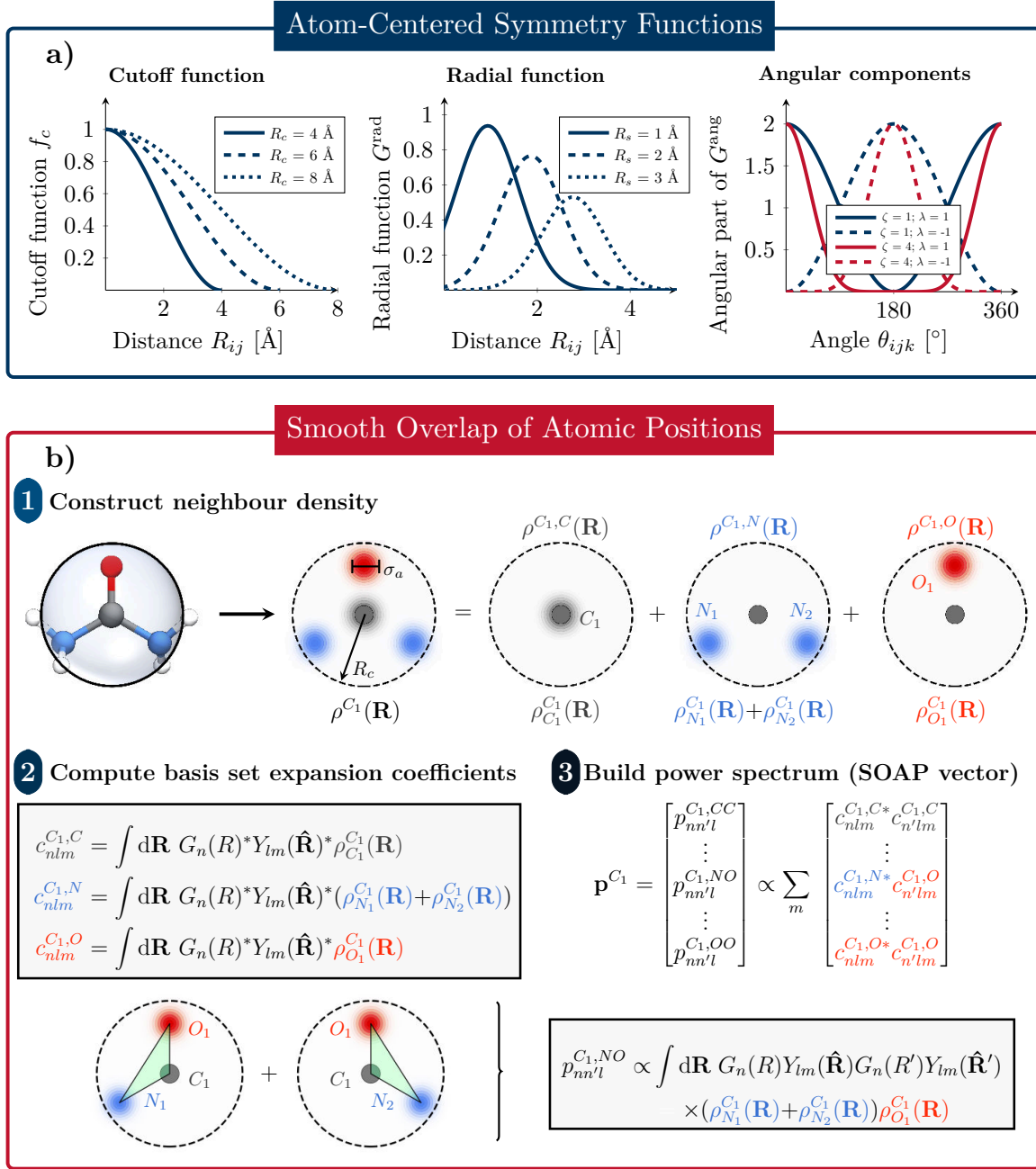


FIG. 2. **Summary of atom-centered symmetry functions (ACSF) and Smooth Overlap of Atomic Positions (SOAP).** a) ACSF: Illustration of the three types of functions relevant for atom-centered symmetry functions. left) Cutoff function with three different cutoff radii. middle) Radial symmetry function with different shifted centers and $R_c = 6 \text{ \AA}$. right) Angular component of the angular symmetry function with different choices for ζ and λ . b) SOAP: Schematic of the smooth overlap of atomic positions descriptor constructed for a non-planar urea molecule. First, atomic positions are transformed into the neighbour density ρ , which is permutationally invariant. Next, ρ is expanded in a local basis of radial functions and spherical harmonics, Y_{lm} . Finally, summing up the square modulus of the expansion coefficients c_{nlm} over the index m provides the rotational invariance power spectrum p .

and thus break the unfavourable scaling, such as done in tensor-reduced atomic density representations.⁶⁶ Furthermore, both types of descriptors discussed above have recently been shown to be incomplete in the sense that they can have trouble differentiating certain arrange-

ments of atoms.⁶⁷ A solution to this is given by descriptors used in moment tensor potentials,⁶⁸ or the more recent atomic cluster expansion (ACE),¹⁷ which both include in principle, higher-order body terms up to infinite order. In practice, they are still truncated after a certain

order, nevertheless making them more complete and adjustable to the system of interest. The ACE approach, which is described in more detail in section IV A, has the additional advantage of allowing for equivariance of the output properties with respect to the coordinates of the system. This enables direct representation of vectorial and tensorial properties, such as dipole moments or polarizabilities, which rotate with the system of interest.

An additional shortcoming in the most literal sense is the restriction to a certain cutoff around each atom, making the resulting descriptors short-sighted. This locality approximation is known to be problematic for cases where long-range effects such as Coulomb interactions are important for the system of interest. They can be included by a suitable baseline, for example by learning partial charges given by reference calculations,^{69,70} or special long-ranged descriptors such as the long-distance equivariant (LODE) framework.⁷¹ Other developments make the descriptors a part of the ML model thus learning them as part of the training process of the model, for example in the context of message-passing neural networks (MPNNs).⁷² Popular examples of these MPNNs include SchNet,²⁷ PhysNet,²¹ and NequiP.²³ While SchNet and PhysNet provide invariant representations of the atomic structure, NequiP introduces a significant innovation by directly incorporating equivariant features that embed rotational symmetry into the model. Furthermore, the recently introduced Allegro model³¹ learns the atomic representation without relying on atom-centred message passing, offering an efficient alternative. We will come back to these ideas in section IV B in more detail.

III. REGRESSION MODELS

After having seen how chemical structure can be encoded based on descriptors, we will next focus on the actual machine learning approaches to relate structural information to the PES. As we are after a description of a continuous property, i.e. energy, we are dealing with a regression task. The simplest way to achieve this would be by linear regression, where the energy E is obtained through a linear relation of the descriptor values G

$$E = \sum_i^{N_{\text{atom}}} \sum_j^{N_{\text{des}}} G_i^j \cdot a_i^j (+b_i^j), \quad (10)$$

summing over all N_{atoms} atoms in the system and all N_{des} associated descriptor values of these atoms. Here, a and b are the only parameters of the model optimised to reproduce the reference energies. In cases where the descriptors are very high-dimensional and sensitive, this can actually give very good representations of the PES after one important modification. If the parameters a and b of the model are chosen to be different for each atom, we are losing the permutational invariance that we painstakingly introduced in the previous section. To illustrate that let us consider a simple system of two atoms: In

this case, the order of our descriptor vectors G_i can't be swapped after the weights have been optimised.

Most MLPs do not rely on relatively restricted linear regression and instead apply more flexible regression models, i.e. models with orders of magnitude more parameters to optimise. Out of these, the most commonly used approaches in the field fall into two broad categories: Artificial neural networks, or kernel-based methods. In the following, both of these regression models will be introduced and we will see how they can be used in MLPs to represent PESs.

A. Artificial neural networks

Artificial neural networks, as one of the prominent models in machine learning, originated as a representation of biological neural networks, but are nowadays a widespread machine learning model capable of reproducing highly complex relations between an input and an output without knowledge about the underlying causation.⁷³ Their functional form is based on a layered structure with connected nodes and associated weights as schematically depicted in Fig. 3. The nodes of the input layer, which hold the provided mathematical description of the input (here: structural information of atoms encoded in descriptor space), are connected via so-called hidden layers to the nodes of the output layer, which after evaluation of the associated functional form contain the information (here: potential energy) that should be associated with the input.

In feed-forward neural networks, which are the most used form for representing PESs, all node values in a layer depend exclusively on the nodes of the preceding layer.⁷³ All of the associated connections hold a corresponding weight a . Additional bias nodes are usually connected to all nodes except the input and serve as an adjustable offset to shift the input of the individual nodes via bias weights b . The functional relation for the evaluation of a node value is essentially a linear dependence on all node values of the previous layer that is further "activated" by a so-called (typically non-linear) activation function as shown on the right side of Fig. 3. The value y_j^i of node j in layer i is then calculated as

$$y_j^i = f_j^i \left(b_j^i + \sum_{k=1}^{n_{i-1}} a_{k,j}^{i-1,i} \cdot y_k^{i-1} \right) \quad (11)$$

implying that only the bias as well as the respective node values and weights of the previous layer contribute to the values of the layer of interest. Here, k is then the index over the nodes in the preceding layer that features n_{i-1} nodes.

The function f_j^i is usually a sigmoid function in the hidden layers, which can be represented as a hyperbolic tangent, and the linear function $f(x) = x$ for the output layer to allow for continuous predictions. The characteristics of a sigmoid function is that it switches in a small

interval from 0 to 1 (or similar) and stays constant outside of that interval. This function is responsible for the great flexibility of neural networks. Without the activation function, the model would feature only highly convoluted linear dependencies with rather poor capability to represent other non-linear functional forms. Due to the activation by the sigmoid function of the gathered linear information from previous layers for each node, neural networks are able to fit arbitrary functional forms and are therefore ideally suited for machine learning. Note that there are also other choices of activation functions such as the rectified linear unit (ReLU) $f(x) = \max(0, x)$, or related variants. In earlier days, these functions were not commonly used as they are not differentiable at all points. However, in recent times they have become a very popular choice in particular, in deep learning applications, given their speed and suitability for graphical processing units.

Predictions with a neural network happen via forward-passing of the input information via the different layers in the neural network. It is important to note, that this functional form can be evaluated very efficiently by the usage of a vector matrix representation of the nodes and weights. Similarly, derivatives of the output can be evaluated efficiently via so-called backpropagation where the partial derivatives are evaluated layer by layer and passed backwards through the network. This enables efficient calculation of derivatives with respect to the network parameters, required for an optimisation of the network, but also with respect to the structural information required for obtaining forces of a PES. Backpropagation is nowadays a standard feature of modern machine learning libraries such as Pytorch or Tensorflow and can be executed with a simple functional call. For further details on neural networks, the reader is referred to Ref. 73, while the application of this model to chemical systems will be presented in the following.

1. High-dimensional Neural Network Potentials

Let us next see how neural networks can be used to represent the PES of a system of interest. In principle, the structural information of each atom is encoded by the descriptors of choice could be used directly as input of a global neural network that would output the potential energy. Such an approach was actually used in early studies of representing PESs with machine learning techniques.^{74,75} However, this results in complications, as the order of the atoms will matter in such a setup. This means that invariance with respect to permutations of atoms is again lost. Furthermore, the complexity of the required model scales very unfavourably with the number of atoms in the system, making this approach unfeasible for larger systems.

Behler and Parrinello managed to incorporate the required structural invariances and break the unfavourable scaling by representing every element of the system by a

separate NN resulting in the so-called high-dimensional neural network potential approach.^{13,35} For this purpose, the total potential energy of a particular configuration is separated into the sum of the contributions of individual atoms to construct the functional relation between the energy as output and atomic configuration as input

$$E_{\text{tot}} = \sum_{i=1}^{N_{\text{atom}}} E_i = \sum_{s=1}^{N_{\text{ele}}} \sum_{i_s=1}^{N_{\text{atom}_s}} E_{\text{NN}_s}(G_{i_s}). \quad (12)$$

Each atomic contribution for a particular element s is represented with a single neural network (E_{NN_s}), shared for all atoms of that element (N_{atom_s}). This also enables systems of different sizes to be represented with the same model, or to apply the trained model to a larger system, as long as the required chemical environments are covered in the training set. In addition, it means that there is linear scaling with the number of atoms in the system, as every atomic contribution can be evaluated independently from the others. A schematic depiction of the resulting representation is shown in the upper part of Fig. 4 for the example of a water slab.

Representing each element with a different NN not only introduced the permutational invariance, but is also an intuitive division of the potential energy as atoms of the same elements are usually more similar than of other elements. However, it is important to note that the resulting atomic energies are not physical as they are simply a tool to reproduce the correct total potential energy. The partitioning is merely a requirement by the locality approximation and a consequence of the fitting and different starting initialisation will result in different atomic energy contributions, as for example shown in Fig. 12.4 of Ref. 76. Nevertheless, there are reports in the literature that showcase the usefulness of atomic energies as an analytical tool and analyse the robustness of local predictions.^{77,78}

This high-dimensional NN scheme is local in that the energy of an atom depends only on the atoms in the close neighbourhood. This is a necessary condition to reduce the effective the dimensionality of the problem, which is intractable otherwise. It is important to note that such a reduction is done in all types of empirical potentials in some way. However, an immediate consequence is the lack of any long-range interactions, such as electrostatics.

Let us summarise this approach once more: A set of descriptors for each element transforms the coordinates of the system to be employed as input for the HD-NNP. These vectors serve as the input for the atomic NNs, which yields the atomic energy contributions that sum up to the total observable as schematically depicted in the upper part of Fig. 4. This functional form additionally allows analytical gradients to be calculated, which is an important feature for molecular dynamics-based sampling techniques. In practice, the values of each symmetry function are usually centred around the average value of the training set and normalised to values between zero and one. This has the advantage that all symmetry func-

tions are on a similar scale and their range falls naturally within the steep region of the activation function, making it easier to find optimal parameters and preventing “saturation” of the network, meaning that most of the hidden nodes have values close to -1.0 or +1.0. Usual architectures for the atomic neural networks in the HD-NNP formalism feature two to three hidden layers with 25 to 40 nodes each. These might seem small compared to other applications of neural networks, but is sufficient in this case due to the choice of suitable descriptors. Nevertheless, other more recent methods feature much larger and deeper neural networks, depending on the system of interest and choice of descriptors. Bias nodes with weight parameters b are also commonly attached to all nodes except those in the input layer. Furthermore, activation functions are not applied in the output layer as this would strongly limit the possible predictive range making it impossible to learn arbitrary potential energy surfaces.

2. Obtaining Analytical Derivatives

In atomistic simulations, forces are generally obtained by computing the negative gradient of the total energy with respect to atomic positions $F_i = -\nabla_i E$. To obtain the force acting on atom i with respect to some Cartesian coordinate α we must apply the chain rule since we have transformed from Cartesian coordinates into symmetry function representations;

$$\begin{aligned} F_{i,\alpha} &= -\frac{\partial E}{\partial \alpha} = -\sum_{i=1}^{N_{\text{atom}}} \frac{\partial E_i}{\partial \alpha} \\ &= -\sum_{i=1}^{N_{\text{atom}}} \sum_{s=1}^{N_{\text{des},i}} \frac{\partial E_{NN_i}}{\partial G_{i,s}} \cdot \frac{\partial G_{i,s}}{\partial \alpha} \end{aligned} \quad (13)$$

using the fact that the total energy E is a sum of atomic contributions E_i from Equation 12 and $G_{i,s}$ is the s^{th} symmetry function of the $N_{\text{des},i}$ symmetry functions for a given atom i .

The first component $\partial E_{NN_i}/\partial G_{i,s}$ depends on the architecture of the atomic neural networks and is obtained from the backpropagation of the partial derivatives through the network. As mentioned above, this can nowadays be efficiently obtained by directly calling a ‘backprop’ function offered by modern machine learning libraries such as Pytorch or Tensorflow. Rewriting Equation 11 for a given layer n we get

$$y^n = f(z_{n-1}(f(z_{n-2} \dots (f(z_1(G_{i,s})))))) \quad (14)$$

where in matrix notation

$$z_i = (\mathbf{b}_i + \mathbf{a}_i^T \cdot \mathbf{y}_{i-1}). \quad (15)$$

The partial derivative of the NN output node with respect to the symmetry functions is then

$$\frac{\partial y^n}{\partial G} = \frac{\partial f}{\partial z_{n-1}} \frac{\partial z_{n-1}}{\partial f} \dots \frac{\partial f}{\partial z_1} \frac{\partial z_1}{\partial G}. \quad (16)$$

The second term $\partial G_{i,s}/\partial \alpha$ depends on the various radial and angular symmetry functions describing the atom. Considering for example the radial component of the ACSF given in Equation 2 the derivative on the central atom i with respect to some coordinate α which can be any of x,y,z component of atoms i or j

$$\begin{aligned} \frac{\partial G_i^{\text{rad}}}{\partial \alpha} &= \sum_j \left[2\eta(R_{ij} - R_s) f_c R_{ij} e^{-\eta(R_{ij} - R_s)^2} \cdot \frac{\partial R_{ij}}{\partial \alpha} \right. \\ &\quad \left. + e^{-\eta(R_{ij} - R_s)^2} \cdot \frac{\partial f_c(R_{ij})}{\partial \alpha} \right]. \end{aligned} \quad (17)$$

It is easy to show from the definition of R_{ij}

$$R_{ij} = \sqrt{(x_i - x_j)^2 + (y_i - y_j)^2 + (z_i - z_j)^2} \quad (18)$$

that

$$\frac{\partial R_{ij}}{\partial x_i} = \frac{1}{R_{ij}} (x_i - x_j) \quad (19)$$

and

$$\frac{\partial R_{ij}}{\partial x_i} = -\frac{\partial R_{ij}}{\partial x_j}. \quad (20)$$

Computing $\partial G_i^{\text{ang}}/\partial \alpha$ is similarly straightforward however more algebraically involved, and so the reader is referred to the SI of Ref. 28. Similarly, the stress tensor, important for the pressure response of a system, can be evaluated analytically via suitable partial differentiation as described in detail in Ref. 54 purely based on pair contributions.

3. Training

After setting up a particular HD-NNP architecture, the model needs to be “trained” to reference points by optimising its parameters in an iterative procedure to reproduce the correct total energies (and forces) of the training set. This is done by minimising a loss function, L , defining the fitness of a model to reproduce the given reference values:

$$L = \frac{1}{2N} \sum_{i=1}^N (E_i^{\text{ref}} - E_i^{\text{model}})^2. \quad (21)$$

Such loss functions can also be augmented by forces, where there is then some freedom about weighting the two types of information. Targeting forces together with energies during the optimization of an MLP usually leads

to much better fits as the forces provide additional information about the curvature of the PES. Furthermore, they are local properties associated with each atom which increases the information content of a single configuration vastly. Training on both energies and forces while retaining energy conservation is possible due to the analytical link between the two properties as shown in the previous section.

Once equipped with a suitable loss function, the weights of the model need to be updated in order to minimise the loss. A simple way to achieve this is local optimisation techniques like steepest descent, where the gradient of the loss with respect to the weights w is followed towards a lower loss

$$w_{\text{new}} = w_{\text{old}} - \eta \frac{\partial L}{\partial w_{\text{old}}}, \quad (22)$$

where η is an adjustable learning rate. Since the loss function is a simple sum over all instances in the training set, these updates can be performed consecutively for each structure. The optimisation process is then usually grouped into so-called epochs, where one epoch means that all structures in the training set were considered once to update a given model. The number of epochs is then another hyperparameter that needs to be chosen by the user.

Usually, a set of test structures, different from the training set, is prepared as well to estimate the quality of the fit. This test set provides an estimate for the transferability to structures not included in the training set. Due to the high flexibility of the model, they can represent rather complex functional relations, but are also prone to overfitting⁷⁹ and have usually many local minima in parameter space. Simple optimiser like gradient-descent-based methods will therefore usually worsen the accuracy of the prediction of the test set after some time. To illustrate this, the typical performance of an ML model during optimisation is shown at the bottom of Fig. 3. While the training points are reproduced better and better in the progress of the optimisation, the high flexibility of the model leads to large fluctuations in between the training points, which can be detected by an increase of the error in the test set.

One method to circumvent these problems is to stop early during the optimisation and carefully monitor the test error for signs of overfitting. In addition, more efficient optimiser such as the adaptive global extended Kalman filter^{28,80} significantly improve the performance of the fitting procedure and help to prevent overfitting from points far away from a given training instance. However, this does not change the fact that many quasi-degenerate local minima are located in the parameter space of the model. It is therefore good practice to perform a variety of fits with different starting conditions to select the set of parameters that is optimal for the training and test set, although this will most certainly still not be the global minimum of the parameters.² Since the model only provides a mathematical representation of the

envisaged relation and can not be used to infer causation, this does not have further consequences.

In contrast, for kernel-based approaches, introduced in the next section, the training procedure is usually more straightforward. In most cases, there exists a closed-form analytical solution which can be directly evaluated to get the global minimum without the need for iterative local optimisation.

B. Gaussian Process and Kernel Ridge Regression

Gaussian process regression (GPR) represents a Bayesian nonparametric regression technique able to approximate complex nonlinear functions of high dimensionality.⁸¹ GPR is similar to kernel ridge regression (KRR) in the sense that they both provide the same type of predictions. However, GPR goes a step further by also giving an estimate of the uncertainty of the prediction, which KRR lacks. Generally, the GPR framework can be derived based on two different approaches, the so-called *weight-space* and *function-space* views. Following closely the excellent review by Deringer and coworkers,³⁷ here we highlight elements from both routes to best communicate the conceptual idea behind using GPR to *learn* the PES of a system of interest based on quantum mechanical reference data.

1. Weight-Space View

In the weight-space view on GPR, we start by approximating the high-dimensional function $y(\mathbf{x})$ as a linear combination of M basis functions, k , centered at representative locations \mathbf{x}_m of the input space, such as:

$$y(\mathbf{x}) \approx f(\mathbf{x}) = \sum_{m=1}^M c_m k(\mathbf{x}, \mathbf{x}_m), \quad (23)$$

where these so-called kernel functions k measure the similarity between two arbitrary data points and c_m are the corresponding coefficients. While the functional form of k does not matter for this derivation, for the sake of illustration, we can imagine Gaussians being placed at the set of representative locations, $\{\mathbf{x}_m\}_{m=1}^M$. This is commonly referred to as the Gaussian or square exponential kernel. It is important to stress, however, that k needs to be symmetric and positive semi-definite. The coefficients, c_m , are then obtained by fitting equation 23 to a training set, $\mathcal{D} = \{\mathbf{x}_n; y_n\}_{n=1}^N$, which corresponds to minimising the loss function

$$\mathcal{L} = \sum_{n=1}^N \frac{[y_n - f(\mathbf{x}_n)]^2}{\sigma_n} + \sum_{m,m'} c_m k(\mathbf{x}_m, \mathbf{x}_{m'}) c_{m'}, \quad (24)$$

where the first term aims to minimise the difference between the data and GPR model and the second term is

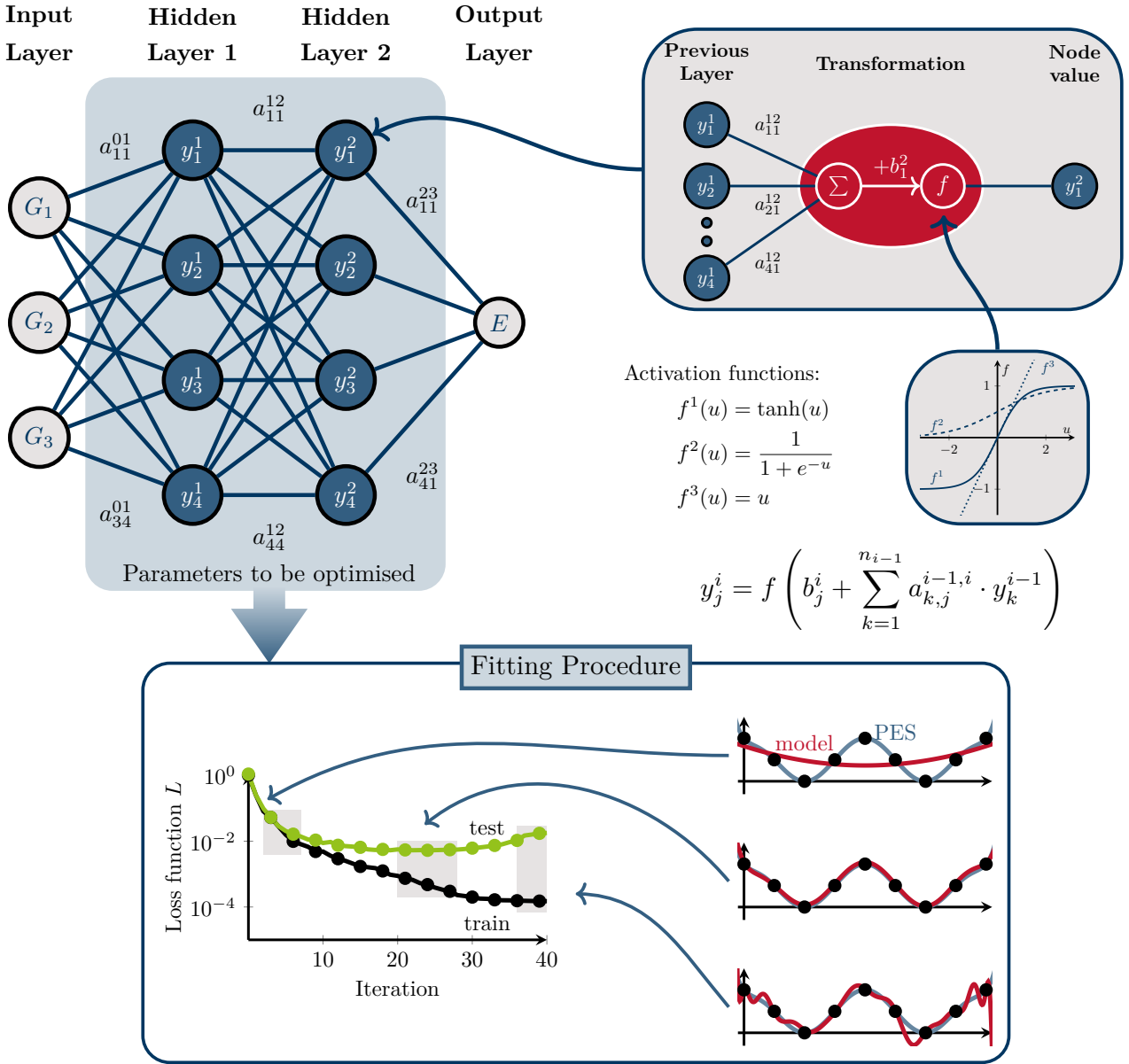


FIG. 3. **Schematic of typical neural network architecture (top) and its typical optimization process (bottom).** Top left: Schematic representation of a neural network with two hidden layers. The output E is obtained as a function of the three input nodes G with four nodes y in each hidden layer. The weights a are represented by lines, while bias weights b are omitted for clarity. Top right: Illustration of the functional dependence of a single node output value on the node values of the previous layer. Bottom left: Illustration of a typical optimization process for a neural network model. Left: Mean error of the training (black) and test set (green) in the progress of the optimization. After substantial improvement of both errors at the beginning of the optimization, the training error usually keeps decreasing, while the test error stagnates or even increases after some time. Bottom right: Corresponding comparison of the reference function (blue) to the neural network model (red) during three representative stages of the optimisation. The neural network is trained to a set of training points of the reference function (black dots) for which the prediction is continuously improved. Due to the high flexibility of the model, regions in between the training points deteriorate after too heavy optimisation.

a (Tikhonov) regularisation to ensure small coefficients, c_m , and prevent overfitting.

The effect of the regularisation can be best understood by remembering that the kernel function k measures the similarity between two points m and m' . If $m = m'$, the value is one and the squared coefficient contributes

strongly to the loss. Minimisation of the loss thus results in keeping c_m small. If we have very dissimilar points (small k), their coefficient would need to be rather large to provide a meaningful contribution to the prediction. However, also this is disfavoured by the regularisation term, thus preventing overfitting.

The parameter σ_n weights the importance of the n th data point and implicitly determines the strength of the regularisation term; choosing σ_n carefully is important to obtain an accurate and smooth GPR model. The result of this is that we effectively interpolate for an unknown point \mathbf{x}_{new} using a linear combination of the most similar representative locations \mathbf{x}_m , given that small similarities will require large coefficients which are suppressed by the regularisation.

To facilitate the next steps, we rewrite equation 24 in matrix notation

$$\mathcal{L} = [\mathbf{y} - \mathbf{K}_{NM}\mathbf{c}]^T \Sigma [\mathbf{y} - \mathbf{K}_{NM}\mathbf{c}] + \mathbf{c}^T \mathbf{K}_{MM}\mathbf{c}, \quad (25)$$

where the Σ is a diagonal matrix of size N with the diagonal elements $\Sigma_{nn} = \sigma_n^2$. The elements of the kernel matrix represent the similarity between each pair of input locations, \mathbf{x}_n and \mathbf{x}_m , as determined by the kernel function, $k(\mathbf{x}_n, \mathbf{x}_m)$. Furthermore, the matrix is symmetric, resulting in $\mathbf{K}_{NM}^T = \mathbf{K}_{MN}$. The coefficients can then be obtained by setting the derivative of the loss function with respect to the coefficients to zero. These are given by

$$\mathbf{c} = [\mathbf{K}_{MM} + \mathbf{K}_{MN}\Sigma^{-1}\mathbf{K}_{NM}]^{-1} \mathbf{K}_{MN}\Sigma^{-1}\mathbf{y}, \quad (26)$$

which can be used to make predictions using the matrix notation of equation 23

$$f(\mathbf{x}) = \mathbf{c}^T \mathbf{k}, \quad (27)$$

with \mathbf{k} being the shorthand notation for the vector of kernel values for \mathbf{x} with respect to the representative points, i.e. $[\mathbf{k}(\mathbf{x})]_m = k(\mathbf{x}, \mathbf{x}_m)$. Unlike artificial neural networks, where weights are typically found through numerical optimisation that usually leads to local minima, the coefficients in equation 26 are derived analytically and represent the global optimum based on the input data, the chosen kernel functions and representative points, and the hyperparameters (both within the kernel function and σ_n). Setting the number of basis functions, M , appropriately is important in GPR. It may seem tempting to place a basis function at every data input location for accurate representation of $y(\mathbf{x})$. With this strategy ($M = N$), known as full GPR, the expression for the coefficients in equation 26 simplifies to

$$\mathbf{c} = [\mathbf{K}_{NN} + \Sigma]^{-1} \mathbf{y}, \quad (28)$$

and the GPR prediction at location \mathbf{x} is given by

$$f(\mathbf{x}) = \mathbf{k}^T [\mathbf{K}_{NN} + \Sigma]^{-1} \mathbf{y}. \quad (29)$$

Full GPR, however, is impractical for large data sets due to the high computational cost and memory demands associated with inverting the matrix \mathbf{K}_{NN} during training (equation 28), scaling as $\mathcal{O}(N^3)$ and $\mathcal{O}(N^2)$, respectively. Once the coefficients \mathbf{c} are fixed after fitting, the inference time for making predictions (equation 27) is determined by the computation of the vector \mathbf{k} and scales linearly

with the number of representative points used, which is $\mathcal{O}(N)$ for full GPR. Therefore, most applications opt for sparse GPR (i.e. $M \ll N$) where the number and location of the basis functions are chosen strategically to balance between accuracy and computational efficiency. In addition to faster inference, sparse GPR also facilitates fitting larger data sets, as the computational costs associated with determining the coefficients (as in Equation 26) scale as $\mathcal{O}(NM^2)$. By now, we have reached the point where KRR and GPR diverge; Although the predictions produced by combining equations 26 and 27 are the same for both KRR and GPR, we will make a short excursion on the function-view on GPR to comprehend how it provides an uncertainty estimate.

2. Function-Space View

In this section, we depart slightly from the review of Deringer et al.³⁷ and present an alternative derivation for the function space view inspired by the comprehensive textbook of Rasmussen and Williams.⁸¹ However, we recommend exploring both derivations for a complete grasp of the involved concepts. In the function-space view, we shift from regarding the estimator $f(\mathbf{x})$ as a fixed deterministic mapping to a probabilistic description through a Gaussian process (GP)

$$y(\mathbf{x}) \approx f(\mathbf{x}) \sim \mathcal{GP}(\mu(\mathbf{x}), \text{Cov}[f(\mathbf{x}), f(\mathbf{x}')]) . \quad (30)$$

A GP is a distribution over functions consistent with data, where any finite set of function values is drawn from a joint (multivariate) Gaussian distribution. This allows us to capture not just a single function but an entire ensemble of possible functions that align with the available data. Before conditioning on data, the GP is fully defined by its mean function, $\mu(\mathbf{x})$, and covariance function, $\text{Cov}[f(\mathbf{x}), f(\mathbf{x}')]$. For the sake of clarity, here we take the mean function to be zero, however, if there is a good guess available, the mean can be subtracted from the observed function values before fitting and added back after prediction. The covariance, conversely, is described by a kernel function, k , which quantifies the similarity between function values at different points:

$$\text{Cov}[f(\mathbf{x}), f(\mathbf{x}')] = k(\mathbf{x}, \mathbf{x}') , \quad (31)$$

ensuring the smoothness of the function f across the input space. The resulting multivariate Gaussian distribution is called the (GP) prior and incorporates our initial assumptions about the functions we are dealing with *before* observing any data. Thus, any admissible function computed at arbitrary locations $\{\mathbf{x}_m\}_{m=1}^M$ is given by the joint Gaussian distribution:

$$\mathbf{f} = [f(\mathbf{x}_1), \dots, f(\mathbf{x}_N)] \sim \mathcal{N}(\mathbf{0}, \mathbf{K}_{MM}) , \quad (32)$$

where \mathbf{f} is the vector of function values and \mathbf{K}_{MM} is a kernel matrix as introduced in the previous section.

Rather than drawing random functions from the prior, we are usually interested in incorporating knowledge from the observations in our training set, $\mathcal{D} = \{\mathbf{x}_n; y_n\}_{n=1}^N$, to make predictions at an unseen location, \mathbf{x}_* . In other words, we are after the conditional probability distribution $P(f(\mathbf{x}_*)|\mathbf{y})$ which is also Gaussian and can be easily constructed from the joint GP prior distribution of the training outputs, \mathbf{y} , and the predicted output at the new location, $f(\mathbf{x}_*)$. In this context, it is important to note that the observed outputs are often considered as noisy versions of the true underlying function values, such that $\mathbf{y} = f(\mathbf{x}) + \epsilon$, where ϵ is independent identically distributed Gaussian noise with zero mean σ^2 variance. Then, the covariance function of two measurements yields

$$\text{Cov}[y_n, y_{n'}] = k(\mathbf{x}_n, \mathbf{x}_{n'}) + \sigma^2 \delta_{nn'} , \quad (33)$$

which we can rewrite in matrix notation as $\mathbf{K}_{NN} + \sigma^2 \mathbf{I}$. Similar to the weight-spaced view, we can employ data-point-specific variances for the noise, σ_n , allowing us to replace $\sigma^2 \mathbf{I}$ with Σ .

Now, the joint distribution of the noisy training outputs, \mathbf{y} , and the prediction, $f(\mathbf{x}_*)$ according to the prior is

$$\begin{bmatrix} \mathbf{y} \\ f(\mathbf{x}_*) \end{bmatrix} \sim \mathcal{N} \left(\mathbf{0}, \begin{bmatrix} \mathbf{K}_{NN} + \Sigma & \mathbf{k} \\ \mathbf{k}^T & k(\mathbf{x}_*, \mathbf{x}_*) \end{bmatrix} \right) , \quad (34)$$

where \mathbf{k} is the shorthand notation for the vector of kernel values for \mathbf{x}_* with respect to the locations encountered in the training data, similar to the definition in the previous section. Then, the conditional distribution of $f(\mathbf{x}_*)$ given the training outputs, \mathbf{y} , is

$$f(\mathbf{x}_*)|\mathbf{y} \sim \mathcal{N}(\bar{f}(\mathbf{x}_*), \text{var}[f(\mathbf{x}_*)]) , \quad (35)$$

with

$$\bar{f}(\mathbf{x}_*) = \mathbf{k}^T [\mathbf{K}_{NN} + \Sigma]^{-1} \mathbf{y} , \quad (36)$$

$$\text{var}[f(\mathbf{x}_*)] = k(\mathbf{x}_*, \mathbf{x}_*) - \mathbf{k}^T [\mathbf{K}_{NN} + \Sigma]^{-1} \mathbf{k} , \quad (37)$$

which correspond to the key predictive equations in GPR which is commonly referred to as predictive distribution. A detailed derivation of conditioning the joint GP distribution on the observations can be found in.⁸¹ Our best estimate of $f(\mathbf{x}_*)$ is then the mean of this distribution, given in equation 36, and associated uncertainty is quantified by the variance in equation 37. As expected, this prediction of the GPR model is equivalent to that obtained in the weight-space view when full GPR ($M = N$) is employed given by equation 29. Interestingly, the variance only depends on the location and similarity of the data points and the noise associated with each point, but not the training set values.

This provides us, in principle, with the necessary tools to perform GPR. However, there is one important aspect related to fitting to quantum mechanical reference data which needs addressing. As seen for HD-NNPs, machine

learning potentials are best setup to estimate an atomic energy function given an atom's local environment, but they are constructed based on electronic structure calculations yielding only the *total* energy and its derivatives, namely the atomic forces and virial stresses. Therefore, some more steps are needed to be able to learn a function when the function's actual values are not available to us, but we have access to its derived properties. We refer the interested reader to the excellent review by Deringer and coworkers for further details [37](#).

3. Gaussian Approximation Potentials

Having covered the general idea behind GPR, let us now apply these concepts to MLPs by discussing the Gaussian Approximation Potential (GAP) methodology developed by Bartok *et al.*¹⁴ As in many conventional and machine learning-based potentials, the key assumption behind GAP is that the potential energy E_{tot} is constructed as a sum of the atomic energies, ϵ_i , such that

$$E_{\text{tot}} = \sum_i^{N_{\text{atom}}} E_i , \quad (38)$$

where N_{atom} corresponds to the number of atoms in the system. An illustration of the resulting structure-energy relation is shown in the lower part of Fig. 4. To account for the distinct energy and length scales of the repulsive and the attractive regime of potential energy surfaces, atomic energies, E_i , are computed based on a linear combination of d -dimensional terms. Most commonly, this involves a two-body (2B) and many-body (MB) term which are both expressed as separate GPR models using suitable descriptors, $\mathbf{q}^{(d)}$, such that

$$E_{\text{tot}} = \delta^{(2B)} \sum_{ij} E^{(2B)}(\mathbf{q}_{ij}^{(2B)}) + \delta^{(MB)} \sum_i E^{(MB)}(\mathbf{q}_i^{(MB)}) , \quad (39)$$

where each term is weighted by the scaling factors $\delta^{(d)}$ which represents an additional hyperparameter. In many GAP models,^{60–63,82} the two-body term makes the largest contribution to the total energy, thus the $\delta^{(2B)}$ is usually set to be five to fifty times larger than $\delta^{(MB)}$. The squared exponential or Gaussian kernel is commonly employed as the kernel function for the low-dimensional 2B term, using the distance between two atoms as a descriptor, resulting in a sparse GPR model using $M^{(2B)}$ representative points. The MB term, conversely, is represented by the SOAP kernel, defined in equation 9, using a set of $M^{(MB)}$ representative configurations resulting in the following expression for the potential energy

$$E_{\text{tot}} = \delta^{(2B)} \sum_{ij} \sum_{m=1}^{M^{(2B)}} c_m^{(2B)} \exp \left[-\frac{|R_{ij} - R_m|^2}{2\theta^2} \right] + \delta^{(MB)} \sum_i \sum_{m=1}^{M^{(MB)}} c_m^{(MB)} (\xi_i \cdot \xi_m)^\zeta , \quad (40)$$

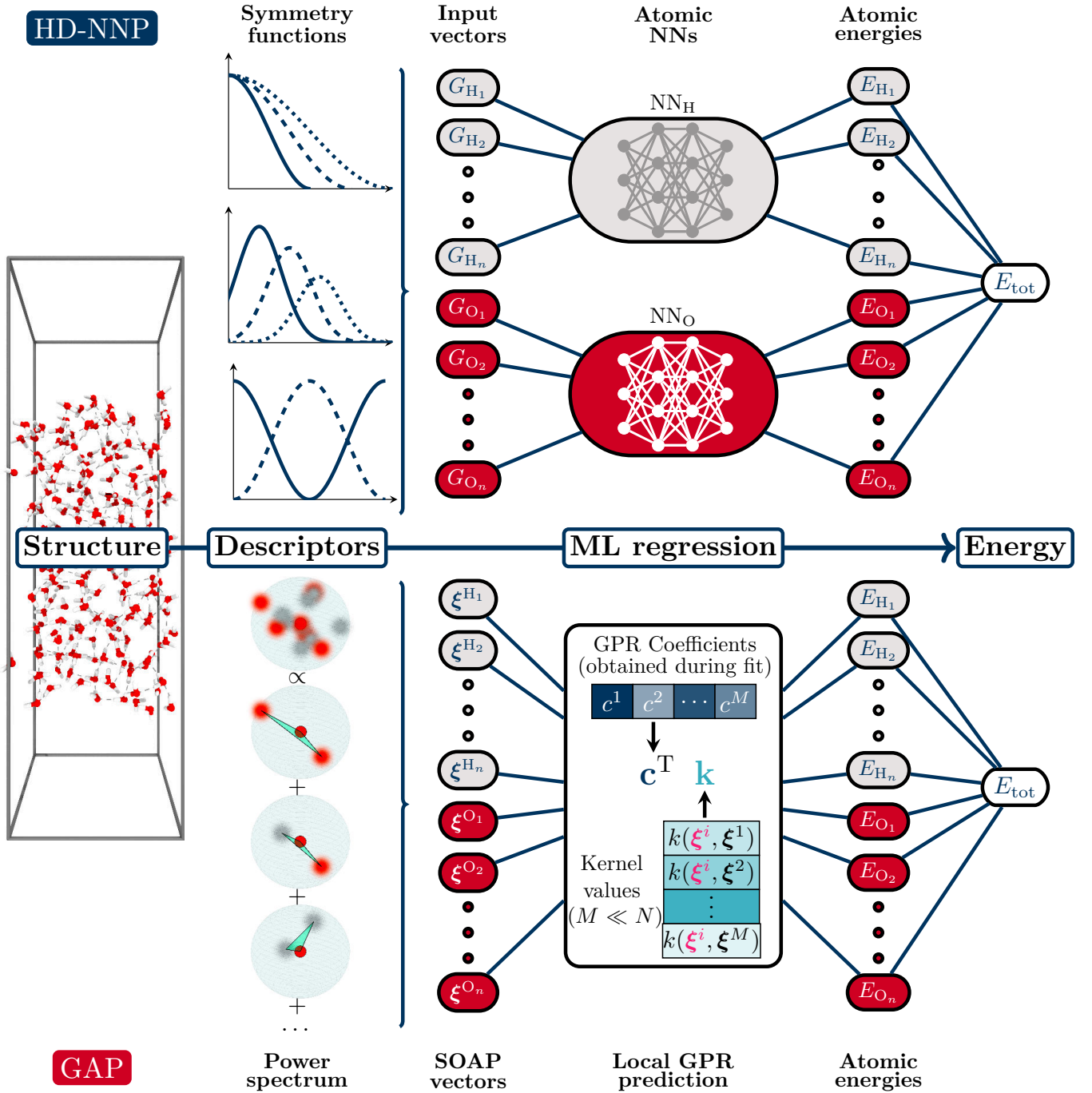


FIG. 4. Representation of the structure–energy relation realised by high–dimensional neural network potentials (HD-NNP, top) and Gaussian approximation potential (GAP, bottom) for the description of a slab of water. In the first step, the structure is transformed either via atom-centred symmetry functions (HD-NNP) or smooth overlap of atomic positions (GAP) into rotationally, translationally, and permutationally invariant vectors. These serve as the input for atomic neural networks (HD-NNP) or local Gaussian process regression models (GAP) to provide atomic energies that sum up to the total energy of the system. This functional relation is analytically differentiable and, thus, can also provide the interatomic forces.

where θ is a hyperparameter related to the 2B descriptor, and ξ is the normalised power spectrum vector as outlined in the SOAP section above. The coefficients of the individual GPR models, $c_m^{(d)}$, are obtained during the

fitting process outlined in the previous section. In order to select the representative points or basis functions for a descriptor, there are different approaches depending on the dimensionality of the descriptor. For low-dimensional

descriptors, such as the 2B descriptor, a uniform grid in the one-dimensional space is chosen to ensure all interatomic distances are well represented, resulting in a relatively small number of representative points, typically less than 100. On the other hand, high-dimensional descriptors, such as the SOAP representation, require a more efficient strategy, such as using the so-called CUR algorithm, which maximises the span of the basis set in a low-dimensional representative subspace of the full descriptor set. The exact number of representative points needed depends on the complexity of the target phase space region the model is being fitted to, and is usually around several thousand.

The regularisers, or data-point-specific variances, σ_n , are an important set of parameters in determining the coefficients, $c_m^{(d)}$, for the GPR model. These regularisers need to be chosen carefully for each data point in the training set, as too large of a value will result in poor agreement with the reference data, while too small of a value can lead to overfitting. It is important to keep in mind that the reference data, such as energies, forces, and stresses, may contain noise due to unconverged electronic structure calculations or other issues related to the *ab initio* reference method.

The inherent approximation of decomposing the potential energy into local contributions also represents a potential bias. The appropriate choice of the regulariser, σ_n , depends on multiple factors such as the property being modelled (energy, force, or virial stress) and the location in the phase space of the configuration. Being closer to the potential energy minimum, solid configurations require more precise fits than liquid configurations, and typical values are ($\sigma_E = 0.001$, $\sigma_F = 0.05$, $\sigma_V = 0.05$) and ($\sigma_E = 0.03$, $\sigma_F = 0.2$, $\sigma_V = 0.2$) for a solid and liquid configuration, respectively, with units of eV/atom for energies (σ_E) and virial stresses (σ_V) and eV/Å for force components (σ_F).

C. Discussion and Outlook of Regression Models

We have now described two routes – HD-NNPs based on artificial neural networks and GAPs based on Gaussian process regression – that relate structural descriptors to forces and energies. These can now be used to extend both the length and time scales of atomistic simulations, with the caveat of any new chemical environments remaining close to those in the training data.

The differences between these two methods can be broadly classified with respect to their descriptors and model complexities. The ACSF descriptors for HD-NNPs are typically low-dimensional descriptors which are then transformed via a highly flexible NN. In contrast, the SOAP descriptors required for the GAP models are of much higher dimension, but this makes the actual regression task ultimately simpler.

These models can be further compared in terms of similarities and differences, as well as their advantages and

disadvantages. A task common to the training of any machine learning model is the judicious selection of the hyperparameters for the model. These need to be chosen before the model training. A combination of experience and systematic testing is the typical approach.

An immediate advantage of the kernel models is that they have an inherent uncertainty estimate available, while NN approaches require additional effort to obtain this. For example, multiple NN-based models can be trained and combined into so-called committee models, where the ensemble variation can provide a powerful uncertainty estimate.⁸³ In terms of computational efficiency, GAP can be expensive for large datasets compared to HD-NNPs. The cost of the regression task scales as $\mathcal{O}(NM^2)$ to compute the coefficients. Evaluation of both HD-NNP and GAP models scale linearly with the number of model parameters but for GAP the number of model parameters is related to the number of representative points in the training data and so overall scales $\mathcal{O}(M)$. This makes NNPs a more attractive option for large and complex (heterogeneous) data sets which require a larger number of representative points. Alternatively, recent developments in another family of methods expand the PES in terms of many-body correlation functions. While both NNPs and GAP rely on low-body order descriptors, moment tensor potentials¹⁵ and the atomic cluster expansion (ACE),¹⁷ are computationally efficient up to high-body order and allow treatment of complex chemical environments involving many different elements. Another general disadvantage of both HD-NNPs and GAP models is the inherent assumption of locality, where the models are truncated at a finite interaction distance. This can lead to significant errors for systems in which intrinsically long-range electrostatic or dispersion interactions are important.⁸⁴ In Section IV, we will discuss methods for overcoming these challenges in more detail.

In the end, the choice of the flexibility in the descriptors and regression model is a smooth scale, ranging from the most extreme cases of having all flexibility in the descriptors as in the ACE¹⁷ that use linear regression, to message-passing NNs^{22,85} that use rather simple descriptors and are introduced in more detail in the next section. In practice, the optimal solution has not yet been found and computational efficiency also needs to be taken into account. A useful way of understanding differences in this respect is by looking at the so-called Pareto front of accuracy-versus-cost achieved with different models. Cost is then usually measured as the time per simulation step using the model, not taking into account the development time and training cost. The best models will provide the lowest cost with the highest accuracy over a large front compared to other available models and architectures. We refer to further aspects on the assessment of the accuracy of a given model in section VI. A notable development towards higher efficiency is the use of graphics processing units acceleration.^{86,87} This is expected to become more and more widespread further pushing the

boundaries of what can be done with MLPs. It is hard to provide a comprehensive recommendation as to which model is best for specific systems. However, the push towards open source and automated development as well as standardised formats and validation tests, as summarised in Tab. S2, enables users to easily compare different architectures. We hope that the overview of current developments as discussed in the next section will provide a good starting point for choosing a suitable model for new work.

IV. CURRENT DEVELOPMENTS

After understanding how the seminal works of high-dimensional MLPs solved the challenges associated with representing PESs, we can now widen the view on the field and look into more recent developments. Overall, these developments either improve upon the chemical descriptors, or the architecture of the regression, targeting improved accuracy, efficiency and generalisation. Another important development is finding an optimum in terms of speed and accuracy. So far the models we have discussed comprise a set of predefined truncated descriptors which are then used as input for a highly non-linear function, the output of which then implicitly contains higher body-order correlations. However many modern MLP approaches instead aim to explicitly capture these correlations.

As previously discussed in earlier sections, integral to all ML models is the consideration of the physical symmetries of the system. In general, all of the properties of a particular atomic structure obey a general symmetry constraint:

$$\phi\{Q \cdot \sigma_i\} = Q\phi\{\sigma_i\} \quad (41)$$

This shows that operating on an atomic configuration ($\sigma_i = r_{1i}, r_{2i}, \dots, r_{Ni}$) with a symmetry operator Q (e.g. translation, rotation) and then taking the ML model output, $\phi\{\dots\}$, should be equivalent to operating on the ML output of the original atomic configuration σ_i and applying the symmetry operation after. In general, different physical properties can transform differently under specific symmetry operations. In atomistic modelling, the focus lies on the Euclidean symmetries (translations, rotations, and reflections) of three-dimensional space, represented by the $E(3)$ group. Since translational invariance is maintained by working with interatomic distances rather than positions, our attention is primarily on rotations and reflections, forming the $O(3)$ group. Upon applying a symmetry operation from this group, a property can either remain invariant or transform equivariantly. For instance, scalar properties such as the global potential energy, which will not change for example if a molecule is rotated (in the absence of an external field), are invariant with respect to $O(3)$ operations. Vectors or higher-order tensorial properties such as forces and

dipole moments, conversely, should obey the same rotation. Also, as previously mentioned in Section II C, the descriptors should be capable of unambiguously differentiating atomic environments, and so should be formally complete.⁶⁷ Recent work can therefore be roughly categorised into four main objectives, 1) generation of a complete set of descriptors, 2) incorporating the representation of the atomic environments directly in the model architecture, which are then another learnable feature, 3) going beyond a local description of atomic environments, and 4) providing generalisable models across large regions of compound space.

A. Completeness of Descriptors

In general, the energy of an atom i can be systematically written as a many-body expansion:

$$E_i = V_1(r_i) + \frac{1}{2} \sum_j V_2(r_{ij}) + \frac{1}{3!} \sum_{j,k} V_3(r_{ijk}) + \dots \quad (42)$$

where each term successively depends on an additional particle.

However, this expansion scales very poorly with increasing leading body order v ($\mathcal{O}N^v$) for N neighbours of atom i within a cutoff and is computationally intractable to go beyond body order $v = 5$. Moment tensor potentials¹⁵ and more recently the atomic cluster expansion (ACE)¹⁷ overcome this issue to give efficient linear-scaling models.^{16,88} Similar to using single particle orbitals in quantum chemistry and building a Slater determinant, ACE generates a basis $A_{iv} = \sum_j \phi_v(r_{ij})$ of one-particle functions ($\phi_v()$) to describe the local atomic environments. This basis is permutationally invariant as a result of summing over all neighbours and is complete. The energy in equation 42 is then constructed from products of these 1-particle basis functions A_{iv} :

$$E_i = \sum_v c_v^{(1)} A_{iv} + \sum_{v_1 \geq v_2} c_{v_1 v_2}^{(2)} A_{v_1} A_{v_2} + \dots \quad (43)$$

$$\sum_{v_1 \geq v_2 \geq v_3} c_{v_1 v_2 v_3}^{(3)} A_{v_1} A_{v_2} A_{v_3} + \dots \quad (44)$$

By averaging the A basis over rotations (see Ref. 17), the total energy can be written as a polynomial of a new rotationally invariant B basis functions:

$$E = \sum_{vi} c_{iv} B_{vi} \quad (45)$$

This resulting polynomial is linear-scaling (\mathcal{N}) irrespective of the body-order of the expansion.⁸⁹ ACE is a complete expansion of the atomic environment and can be used as a framework to classify other types of potentials. For example, moment tensor potentials introduced already in 2016¹⁵ are also a complete basis spanning the space of atomic environments and have a 1:1 mapping to ACE.⁹⁰

B. Learnable Descriptors: Graph Neural Networks

So far, all of the MLP models have been based on (systematic and complete in the case of ACE and MTPs) fixed descriptors of the local atomic environment. However, another class of MLPs are based on the well-established field of graph neural networks (GNNs), where the representation can be learned from molecular graphs. GNNs exploit the fact that, in general, atomic environments are highly amenable for representation as graphs, where nodes (atoms) are connected to all other nodes (within a cutoff) via edges e_{ij} . For the successful subclass of message-passing neural networks (MPNNs), each atom/node i is associated with a latent state h_i , updated with each message-passing iteration t . A message m_i^{t+1} is constructed on a node i by ‘pulling’ information of the states from all neighbouring atoms $N(i)$ using a message function M_t :

$$m_i^{t+1} = \sum_{j \in N(i)} M_t(h_i^{(t)}, h_j^{(t), e_{ij}}) \quad (46)$$

The state of each node is then updated based on these messages

$$h_i^{t+1} = U_t(h_i^t, m_i^{(t+1)}) \quad (47)$$

where U_t is a learnable node update function.

Early architectures such as SchNet²⁷ and Dimenet⁹¹ were based on invariant features h_i . This guarantees that the predicted energy will be invariant under the symmetry operations described. More recent MPNNs are instead based on vectorial or tensorial representations at each node. These models include NequIP,²³ PaINN,⁹² NewtonNet,⁹³ and SEGNN.⁹⁴ Coupling these ideas with attention and transformer-like concepts leads to another class of models.^{95–98} All these architectures are inherently *equivariant* with respect to the relevant symmetries of rotation, translation and inversion (E3 symmetry group). Such equivariant MPNNs are much more data efficient since the relevant symmetries are already encoded in the model, and therefore large amounts of data are not required to ‘learn’ these equivariances and have greater accuracy. Unlike the NNP and GAP models discussed in previous sections, which strictly contain local chemical information, MPNNs can propagate semi-local information via iterative message-passing steps. Thus, the so-called ‘receptive field’ $r_{c,e}$ of an MPNN is expanded beyond the local atomic cutoff $r_{c,l}$ based on the number of message passing layers N : $r_{c,e} = N_t r_{c,l}$. Information about increasingly non-local features can be built up through multiple message-passing layers t . However, this expanded receptive field of equivariant MPNNs leads to a significant scaling problem, making parallelisation involving multiple message-passing steps very difficult since there is a cubic scaling of the number of neighbouring atoms with the number of message-passing steps. For example Ref. 99 shows that an MPNN for bulk water with a local cutoff of 6Å containing 96 neighbours increases to

20834 upon 6 message passing steps. This highlights that maintaining the locality of the model is highly desirable to allow for efficient implementation of these methods.

The relationship between overall body order of the features h_i and message passing has been explored in several recent works.^{100–102} While the previous equivariant models discussed exploited message passing, they only considered 2-body messages, resulting in lower efficiency due to the increased message-passing steps required to capture many-body correlations. The most recent state-of-the-art methods – Allegro⁹⁹ and MACE²⁰ – thus combine message passing with high body order features. For MACE, each layer now comprises many-body messages, resulting in efficient potentials that can be systematically expanded to arbitrary body-order, thereby explicitly including higher-order correlations, without requiring the many message passing steps of previous MPNNs (typically 2 compared to 6).²⁰ MACE has recently been shown to provide convincing accuracy across application in many diverse areas.¹⁰³ Other MPNNs have been very useful for universal potentials across the periodic table.¹⁰⁴ In summary, MPNNs are accurate, data-efficient, and fast and are expected to be at the forefront of next generation MLP applications and developments.

C. Beyond Locality

While elemental systems and those with significant screening effects¹⁰⁵ can be successfully treated with short-range models, such models can fail for systems governed significantly by long-range electrostatic or dispersion interactions. Therefore the inherent locality assumption of MLPs – required to facilitate practical implementation – is a major shortcoming. Some models include physically motivated corrections – similar to DFT – for example, PhysNet²¹ and Tensormol¹⁰⁶ use Grimme’s DXX family of dispersion corrections.¹⁰⁷ However, many approaches to address this issue are based on a decomposition of the total energy as a sum of short-range terms E_{sr} and long-range E_{elec} contributions:

$$E_{tot} = E_{sr} + E_{elec} \quad (48)$$

The most straightforward approaches simply involve subtraction of the long-range electrostatic component using a standard Ewald-like sum^{14,108} and subsequently training a purely short-range model to the difference. However, this assumes fixed charges and also raises the question of what is the correct partial charge to assign to the atoms. This can be addressed by exploiting machine learning to address the electrostatic component, thereby training two models for the short and long-range components. So-called 3rd generation MLPs account for environment-specific charges, by training an additional NNP to predict the atomic charges or higher order multipoles as a function of the chemical environment.^{21,69,85,106,109–112} These models aim to reproduce reference partial charges on atoms in a system,

which are then used in an Ewald summation to compute the long-range energy contribution. Since charges are not a quantum mechanical observable, some charge partitioning schemes should be used on the electronic structure calculations to obtain the reference charges. Examples include Hirschfeld and Bader charges or from dipole moments – however, it should be noted that the choice of charge partitioning scheme is not unique. These are then subtracted from the reference energies and forces so to avoid double-counting portions of the long-range term, and a standard HDNNP is trained to give the short-range contribution E_{sr} . While this third-generation NNP approach has been successful in capturing long-range and even dispersion interactions, there is still an issue in describing non-local effects.

There are many cases in chemistry and biology in which there is a global change in the electronic structure such as long-range charge transfer or when a system has multiple charge states, which occur outside of the local chemical environment considered by the cutoff or message passing steps. For example, protonation/deprotonation of a molecule overall results in a change in the total charge of the system. Other situations for example in surface science where dopants far from the adsorbate influence adsorption geometry and binding again require a model that can faithfully capture interactions which extend far beyond the typical cutoff. So-called 4th-generation models thus use atomic charges based on the global charge of the system. A charge equilibration scheme⁷⁰ redistributes the charge density over the system to minimise the total electrostatic energy. Similar to equation 48, the total energy is again split into short and long-range contributions, however now the short-range part contains non-local charge information obtained via charge equilibration:

$$E_{total}(R, Q) = E_{elec}(R, Q) + E_{short}(R, Q) \quad (49)$$

Other promising models are based on a more global approach such as the long-distance equivariant representation (LODE),⁷¹ where non-local information is explicitly incorporated into the feature descriptors and symmetric gradient-domain machine learning (sGDML)¹¹³ which directly learns the forces to give an energy-conserving global model.

D. General Purpose and Foundational Models

Another very promising recent development is the establishment of MLPs that are applicable throughout chemical compound space by training on very large and diverse datasets. Initially, such attempts were mostly limited to property predictions and minimum energy structures since achieving robust and accurate force and energy predictions for stable simulations had been prohibitively difficult. For deeper insights into the concepts of property predictions across chemical compound space, we refer the interested reader to the expert review by

Huang and von Lilienfeld⁴³. Earlier attempts at generalisable representations of PESs have concentrated on relatively well-defined regions of compound space, such as elementary systems like carbon,⁶² or silicon¹¹⁴ showcased in section VII in more detail.

The recent progress in model architectures, data curation, and training algorithms has led to recent successes in delivering MLPs that provide stable simulations across very diverse systems and beyond their training domain. Examples of these advanced models include MACE-MP-0,¹¹⁵ MACE-OFF,¹¹⁶ GNoME,¹¹⁷ MatterSim,¹¹⁸ and CHGNet.¹¹⁹ These models make a promise of being foundational models for molecular and materials modelling. They have demonstrated the capability to generalise well beyond the systems they were initially trained on, enabling accurate and reliable simulations for a wide range of chemical compounds and materials. One of the significant advancements contributing to this success is the development of more sophisticated neural network architectures that can capture the intricate details of inter-atomic interactions. Additionally, the creation of extensive and high-quality training datasets, such as the MPtrj dataset,¹¹⁹ which encompass a broad spectrum of chemical environments, has been crucial. This comprehensive data helps the models to learn more generalised features, leading to improved performance across various types of compounds. Moreover, the improvement in training algorithms, including techniques to prevent overfitting and methods to ensure the physical plausibility of the predictions, has further enhanced the robustness of these models.

Another very promising direction of this research is the possibility for fine-tuning the model to new training data and other reference methods by utilising the concepts of transfer learning. Techniques like transfer learning, or delta learning can be employed effectively, where a pre-trained model is fine-tuned with new training data or adapted to different reference methods, thus extending its applicability and improving its accuracy for specific tasks. This approach allows the foundational models to be adapted for specialised applications, making them incredibly versatile and powerful tools for the molecular and materials modelling community. By continuously integrating new data and refining their algorithms, these models are expected to evolve, providing even greater accuracy and efficiency in simulations, ultimately accelerating the discovery and development of new materials and chemicals.

V. DATA SET GENERATION

After having seen how a robust and accurate representation of the PESs can be achieved with both kernel and NN-based methods, we will now concentrate on the generation of representative data sets. Each machine-learning model is only as good as its underlying data. Thus, special care should be put into curating represen-

tative and well-balanced data. In addition, reference calculations can become expensive — in particular when thinking of correlated wavefunction methods — so additional emphasis should be put on keeping data sets compact.

When thinking about this task, one might simply start out with generating random configurations and computing their energies (and forces) with a suitable reference method, such as DFT. However, in most cases, this will result in very unfavourable structures, so some physical sampling in preparation for the data set generation is usually advantageous. This can either be done by molecular dynamics or any other sampling technique applicable to the specific system of interest. Generally, the optimal approach will depend on the application the user has in mind and can vary significantly from system to system. For instance, including data corresponding to local minima of the PES will be crucial for the model to reliably predict the equilibrium configuration of a solid while data at higher temperatures will be required to describe a liquid phase. Next, one might start selecting a random sample from the previously sampled pool of configurations, thus generating a Boltzmann-weighted distribution. These random sampling techniques, and also other hand-crafted selection methods, can in many cases result in a decent first model, but remain relatively ad hoc. Overall, it is usually quite easy to generate new configurations, but it is a much harder task to select the “right” ones.

Fortunately, there are multiple strategies to generate data sets in a more data-driven and automated way which will be presented in the following sections. These can be roughly categorised based on which side of the structure-energy relation they are operating on. There are multiple strategies that rely on structural similarity measures to select new configurations to be added to the data set. Furthermore, so-called uncertainty based techniques can be used to select points where the model shows a high uncertainty in its prediction.

A. Structural Selection Techniques

A popular similarity-based selection technique is farthest point sampling (FPS),^{3,120} which is a greedy algorithm that selects the structure that is most different from the previously chosen structures, in order to create a structurally diverse training set. To measure the similarity between two structures, A and A' , FPS employs local representations $\mathbf{q}_i^{(d)}$ to describe the atomic environments in d -dimensional descriptor space, such as those discussed above. The most intuitive approach to use these local descriptors to compare and match entire configurations by averaging the individual representations $\mathbf{q}_i^{(d)}$ over all atoms in each configuration, resulting in a mean representation of each structure, $\bar{\mathbf{q}}^{(d)}$. By comparing $\bar{\mathbf{q}}_A^{(d)}$ and $\bar{\mathbf{q}}_{A'}^{(d)}$, the topological difference between the config-

urations A and A' can be quantified. This similarity is represented by a distance, L , and FPS selects configurations such that the distance between a new configuration, $\bar{\mathbf{q}}_{m+1}^{(d)}$, and all previously chosen structures in the database, $Q_{\text{chosen}} = \{\bar{\mathbf{q}}_1^{(d)}, \bar{\mathbf{q}}_2^{(d)}, \dots, \bar{\mathbf{q}}_m^{(d)}\}$, is maximized, as shown in the equation:

$$\bar{\mathbf{q}}_{m+1}^{(d)} = \operatorname{argmax}_{\bar{\mathbf{q}}^{(d)}} [L(Q_{\text{chosen}}, \bar{\mathbf{q}}^{(d)})], \quad (50)$$

where $\bar{\mathbf{q}}^{(d)}$ is the structurally averaged descriptor for all configurations in the pool of potential training structures. It is possible to use different distance metrics L such as the summed Euclidean distance of the query points to all points in the existing data set. The SOAP descriptor is particularly useful in this context as the dot product of two independent SOAP descriptors corresponds directly to the overlap and structural similarity.¹²¹ However, other descriptors such as ACSFs can also be used as long as sufficient distance measures are introduced.

Another technique that operates directly on structures is normal mode sampling.¹²² Here, new structures are generated by using the normal modes of an equilibrium geometry to generate distorted structures along the normal modes according to the thermal harmonic oscillator distribution. This technique has recently been extended to consider structures along reaction pathways in so-called transition tube sampling.¹²³

B. Active Learning

The main advantage of machine learning approaches over traditional functional forms is their flexibility and the possibility for iterative improvement. While low dimensional potentials in general do not have to become better after a certain point when more reference data is taken into account, machine learning models will gradually improve, if additional data is included in the fitting procedure. Due to the flexibility, however, structures far away from any point in the training set are not well represented and are therefore prone to extrapolation errors.¹²⁴ The set of structures used for the training therefore has to reflect the relevant configurations encountered in the subsequent application. In general, two different scenarios for extrapolation problems are possible.

The first problematic situation is a region that is beyond the boundary of the configuration space spanned by the training set as sketched on the left side of Fig. 5. If in such a situation the structure is very far away from the boundaries, the model loses all its predictive power, due to the absence of physical insight. These situations are fortunately easy to detect by comparing the descriptors of a configuration in question to the range of values encountered in the training set. If any descriptor is outside of this range the new structure suffers from extrapolation and will most likely not be represented with sufficient quality. The second case in which MLPs will not

provide plausible predictions is for regions that are underrepresented in the training set as shown on the right side of Fig. 5. These cases are much harder to detect for a single model, but can be prevented by appropriate preparation of the training set to avoid holes. In addition, two models fitted with different starting parameters will provide very different predictions in such a region, due to the large quantity of local minima in parameter space. By comparison of the prediction of two slightly different models it is therefore possible to detect exactly such regions without ever inquiring the usually expensive reference method. Gaussian Process based models can easily identify both situations using their intrinsic error estimate that will flag regions far away from any other data.

At first, the poor capability of machine learning models for extrapolation might look like a significant drawback of these methods, since any transferability to unknown situations is lost and predictions become useless. But at the same time, these properties allow for very powerful strategies to improve the description of the model and automate the process of assembling the reference set. As shown in Fig. 5, when points are iteratively added to the training set that have been detected to be either outside the boundaries or in underrepresented regions of the configuration space spanned in the training set, these regions can be selectively improved. If combined with a physically motivated sampling of the underlying PES, this can be used to generate structure-energy relations in an unbiased and highly efficient way.

These concepts can be generalised under the framework of active learning, where the most suited configurations for an improvement of the model are added to the training set.^{125–133} The term originates from the idea that the learning algorithm can interactively query an “oracle” to label new data points with the desired outputs. This is usually done by having access to some kind of uncertainty estimate, allowing to filter large sets of potential candidate structures which do not have to be labeled with the respective reference method. One can then design iterative procedures which cycle through the steps of 1) getting an uncertainty estimate for a large pool of candidate structures, 2) selecting and labelling a small set of structures with the highest uncertainty, and 3) training an improved model.

In the context of neural network based MLPs, a single model usually not provide an uncertainty estimate (although there are architectures where this can be achieved^{134,135}). However, we have seen that comparing the prediction of two slightly different models can provide us with an indication of uncertainty. This can be formalised in so-called ensemble or committee models, where multiple HD-NNPs are combined and the committee members are separately trained from independent random initial conditions to a subset of the total training set.⁸³ While the committee average provides more accurate predictions than the individual HD-NNPs, the committee disagreement, defined as the standard deviation

between the committee members, grants access to an estimate of the error of the model. This committee disagreement provides an objective measure of the error of the underlying model.¹³⁶ To construct a training set of such a model in an automated and data-driven way, new configurations with the highest disagreement can be added to the training set. This is an active learning strategy called query by committee (QbC) and can be used to systematically improve a machine-learning model.^{137,138} This has been utilised extensively in recent times for the automated development of NNPs for various systems. As seen above, MLPs based on GPR have a built-in uncertainty estimate and can be used for similar active learning strategies.

C. Reinforcement Workflows

The above-described data-driven techniques for the selection of new points to be added to a training set enable the user to establish workflows for the improvement of an MLP. It has become standard to train an initial model, which is subsequently reinforced to better reproduce user-selected and problem-specific properties, or expand into regions of phase space that were previously not part of the training data. Initial models can often be used as very effective structure generators, thus preventing the requirement for expensive reference calculations during sampling. Either structure-based, or uncertainty-based criteria, or a combination of both are then used to filter the large set of structures and label the data. Recent developments have shown that it is possible to use the uncertainty estimate of MLPs either to stabilise a simulation in regions further away from the existing data,⁸³ or bias simulations towards higher uncertainty for quicker exploration of configuration space.^{139,140} The latter has been introduced under the term “hyperactive learning” as it enables faster generation of configurations for an improvement of the model.

VI. VALIDATION

After having seen how structure-energy relations can be represented with MLPs and how data sets can be assembled, we need to focus on the validation of the resulting model. This is one of the most important steps in the development of a new model in order to verify that we can trust the predictions of the MLP. For this tutorial, we will mostly focus on two types of validation steps, numerical errors with respect to the “learned” properties, and secondary properties derived from the representation of the PES. For further details, we refer the interested reader to Ref. 141 which provides an excellent detailed introduction to this topic.

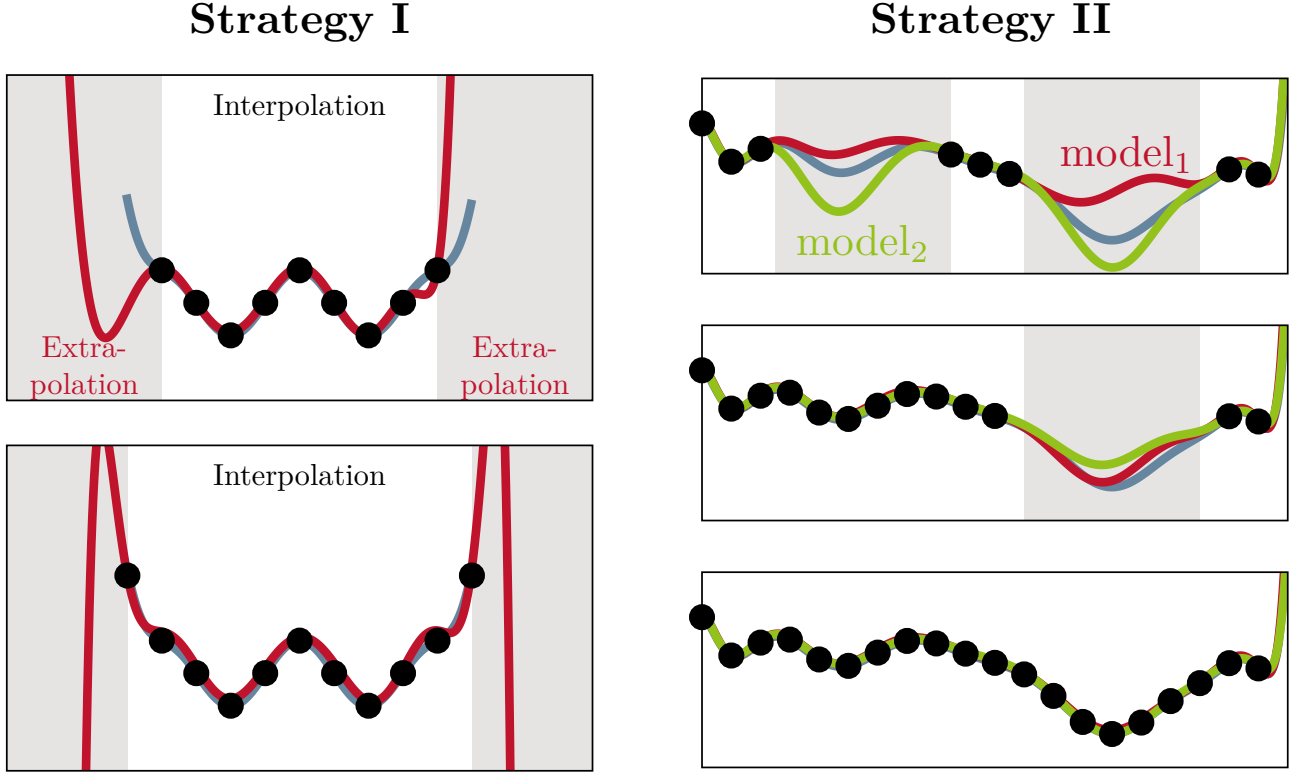


FIG. 5. Representation of two general strategies for an improvement of a machine learning potential applicable to both neural network and Kernel-based approaches. Left: Improvement of the boundaries of the reference set can be achieved by adding structures that were detected to leave the range of descriptors encountered in the training set. Right: Regions that are underrepresented in the training set can be improved by adding structures to the training set for which two slightly different models provide diverging predictions. The reference potential energy surface is shown in blue, the machine learning models in red and green, and the training points of the reference function are depicted as black dots. Regions that are not well represented by the model are highlighted in grey.

A. Primary Properties and Numerical Errors

A starting point to assess the performance of a machine learning model is to use metrics like Root Mean Squared Error (RMSE) and Mean Absolute Deviation (MAD) for the primary properties of the model. These are the reference energies E and forces F that the model is trying to reproduce directly. RMSE is a commonly used metric that measures the average difference between predicted and actual values. It is calculated as the square root of the average of the squared differences between the predictions and the actual values, e.g. for energies E

$$E^{\text{RMSE}} = \sqrt{\frac{1}{N} \sum_{i=1}^N (E_i^{\text{ref}} - E_i^{\text{model}})^2}. \quad (51)$$

This metric is sensitive to outliers, meaning that large errors in a small number of samples can have a disproportionate impact on the overall score.

On the other hand, MAD measures the average absolute difference between predicted and actual values, without taking into account the direction of the error

$$E^{\text{MAD}} = \frac{1}{N} \sum_{i=1}^N |E_i^{\text{ref}} - E_i^{\text{model}}|. \quad (52)$$

This metric is less sensitive to outliers, making it usually a good choice for cases with extreme values. However when employing an MLP in simulations, bad predictions for a small set of outliers can severely deteriorate the quality of the sampling. It is therefore usually more revealing to report RMSE values rather than MAD.

Overall, both RMSE and MAD are commonly used in machine learning to validate the performance of a model and to compare different models. Using these metrics is a good starting point for validating a machine learning model and ensure it is able to accurately predict the reference data it was trained against. The best practice is also to compute them for an independent validation set rather than only for the training or test data. This makes sure that no underlying bias in the selection of the training

data is skewing these performance metrics. However, it is important to keep in mind that these measures should be used in conjunction with other validation techniques to ensure that machine learning models are performing as expected and are able to accurately predict chemical properties.⁸⁹ Furthermore, users need to develop a feeling for the actual values of the error measures for a given system and how they translate into actual performance in simulations is not always clear. As a rule of thumb, energy errors below 1 meV (≈ 0.025 kcal/mol ≈ 0.1 kJ/mol) per atom and force errors of 100 meV/Å (≈ 2.5 kcal/molÅ ≈ 10 kJ/molÅ) or lower are usually desirable. Furthermore, the use of relative errors with respect to the learned observable enables better comparison over the full range of values and makes it easier to compare different systems.

B. Validation of Secondary Properties

While numerical errors can usually give a good initial assessment of the quality of a developed MLP, it is important to validate the prediction of the model more rigorously for the performance in atomistic simulations. After all, we want to use our model to predict physical quantities, and therefore other secondary properties derived from the representation of the PES need to be tested with respect to the reference method. These are usually system and application-specific, requiring some degree of domain knowledge. It is therefore common to design a suite of validation tests for the particular question at hand in order to build trust in the predictions with the model. Nevertheless, these tests can broadly be categorised into structural and dynamical properties.

One example of a structural property that is commonly analysed is radial distribution functions (RDFs).¹⁴² RDFs are defined for pairs of atom types and describe how density varies as a function of distance from a reference particle. It is computed by counting the number of particles dn_r within a shell of thickness dr

$$g(r) = \frac{dn_r}{4\pi r^2 dr \cdot \rho^N} \quad (53)$$

divided by the spherical shell volume times the number density ρ^N . $g(r)$ is related to many other static properties such as the structure factor, or the potential of mean force and thus gives a very good overview of the structural properties of a system. Given its pair-wise nature, it should only be considered as the minimum condition in the validation of an MLP, and it is usually important to check higher-order structural properties such as angular or dihedral distributions.¹⁴³

Dynamical properties include diffusion constants, the phonon spectrum of solids, or more generally the vibrational density of states (VDOS), as well as IR or Raman response of a system of interest. Given the additional complexity of predicting the latter two observables due to the need for dipole moments and polarisabilities, it is

usually sufficient to evaluate the predictive power of an MLP with respect to the simpler VDOS. It can be obtained from the Fourier transform of the velocity-velocity autocorrelation function and can be readily dissected into atom-wise components to give a more resolved overview. The frequency dependent VDOS $G_\alpha(\omega)$ for species α is then given by

$$G_\alpha(\omega) = \mathcal{F}(\langle v_\alpha(0) \cdot v_\alpha(t) \rangle), \quad (54)$$

where \mathcal{F} denotes the Fourier transform of the autocorrelation function for velocities v from time 0 to t as ensemble average $\langle \dots \rangle$. Spanning the whole range of possible dynamical processes in a system of interest from slow translational and librational motion, up to bending and stretching modes, the VDOS is a great summary of the performance of a model for dynamical properties. Example code to obtain both RDFs and VDOS is available in our Colab tutorial.

In many cases, the actual properties of interest for a system under investigation are too expensive to be validated explicitly with the reference method. This is one of the main purposes of using machine learning for atomistic simulations in order to push the boundaries of what is doable with existing methods. In such cases, sufficient trust in the model has to be obtained based on cheaper and simpler properties. Having access to an estimate of uncertainty during the simulations, such as given by the above-mentioned committee methods, or Gaussian process regression, can further help to validate predictions for system sizes too large or simulation times too long to be treated with the reference method.

Finally, the prediction of a model can also be compared to experimental observables. This is particularly suitable for cases where the observable cannot be easily obtained with the reference method, thus providing not only an assessment of the model's performance, but also of the underlying electronic structure method and sampling technique. At the same time, it does deviate slightly from the pure assessment of the MLP, as factors such as suitability of the reference method and approximations in obtaining the observable also contribute to this comparison. Examples of this can be finite size effects in atomistic simulations, limited statistics, but also underlying approximations such as linear response theory. Nevertheless, a comparison to the experiment can be understood as the Holy Grail of validating simulations from first principles and should always be part of a well-designed validation procedure.

An example for the validation of an MLP for primary and secondary properties is shown in Figure 6. It is for a developed neural network based model of a solvated fluoride ion by water as shown in panel a. Numerical errors of the force prediction with respect to the reference DFT method are given in panel b, while structural properties (RDFs) and dynamical properties (VDOS) are validated in panels c and d. This example shows a well-developed model where reference and prediction agree to a satisfactory degree.

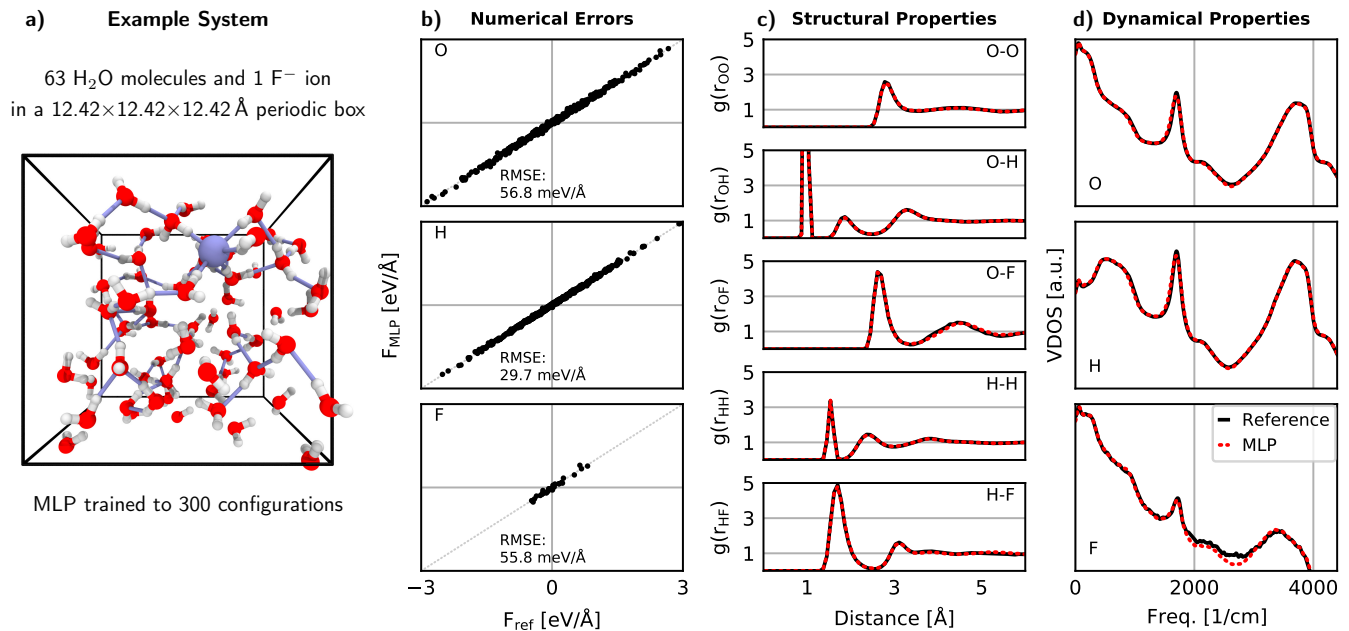


FIG. 6. **Example of the validation of an MLP for the description of a fluoride ion in water.** a) Overview of the system of interest and trained MLP. b) Analysis of the numerical force errors of the MLP. The correlation of the reference force and prediction is shown for each element in the system together with the force RMSE. c) Performance of the MLP for structural properties encoded by the Radial Distribution Functions (RDFs) for all pairs of elements in the system. d) Performance of the MLP for dynamical properties as provided by the Vibrational Density of States (VDOS) for each element in the system. VDOS are shown in logarithmic scale to facilitate easier comparison over the full frequency range. Figure adapted from Ref. 144.

VII. SHOWCASE EXAMPLES

In the last part of this tutorial, we will look at some showcase examples that highlight what can be done with the machine learning techniques discussed above. We will give an overview of different applications that rely either on kernel-based or neural network based MLPs in combination with density functional theory and modern sampling techniques. While impressive new developments with foreseeable high impact are ongoing as described in detail in section IV, we concentrate here on examples that highlight the transformative power of MLPs to provide new scientific insight. This has mostly been delivered by the two first established techniques of HD-NNPs and GAP, which is why we dedicate a larger proportion of the examples to these methods to best showcase the state of the art of applications.

In the last few years, GAP models have been very successful in providing general-purpose potentials for elementary systems. The first set of examples highlights two cases for this particular application and are given in Figure 7 a) and b). The first one is a general-purpose model for carbon,⁶² able to describe the rich allotropy of carbon including diamond, graphene, graphite, nanotubes, and fullerenes. Furthermore, it is also applicable to amorphous and liquid phases, relevant for various

technological applications. The model describes the relative stability of these different polymorphs at a level of accuracy not achieved before with force fields. This has enabled studies of graphene rippling behaviour and its dependence on defects in the material.¹⁴⁵ The second is on work using a general purpose GAP model of silicon to reveal new phase transition behaviour when compressing silicon at high pressures.¹¹⁴ Although not included in the training process of the model, it was able to faithfully reproduce a previously unknown transient phase observed before crystallisation.

The second set of examples at the bottom of Fig.7 highlights another flavour of machine learning for atomistic simulations, which is more tightly coupled with *ab initio* sampling codes. The general idea is that enabled by a robust uncertainty estimate in the MLP, it is possible to train the model ‘on the fly’ during sampling using a reference method and switching to the model once it is accurate enough. This drastically reduces the number of reference calculations and speeds up the sampling.^{148–151} The bottom row of Fig. 7 shows two applications of this approach, first to describe the phase behaviour of silver iodide¹⁴⁶ (Fig. 7 (c)), and second for finding global minima of various compounds,¹⁴⁷ while substantially reducing the number of required reference calculations (Fig. 7 (d)).

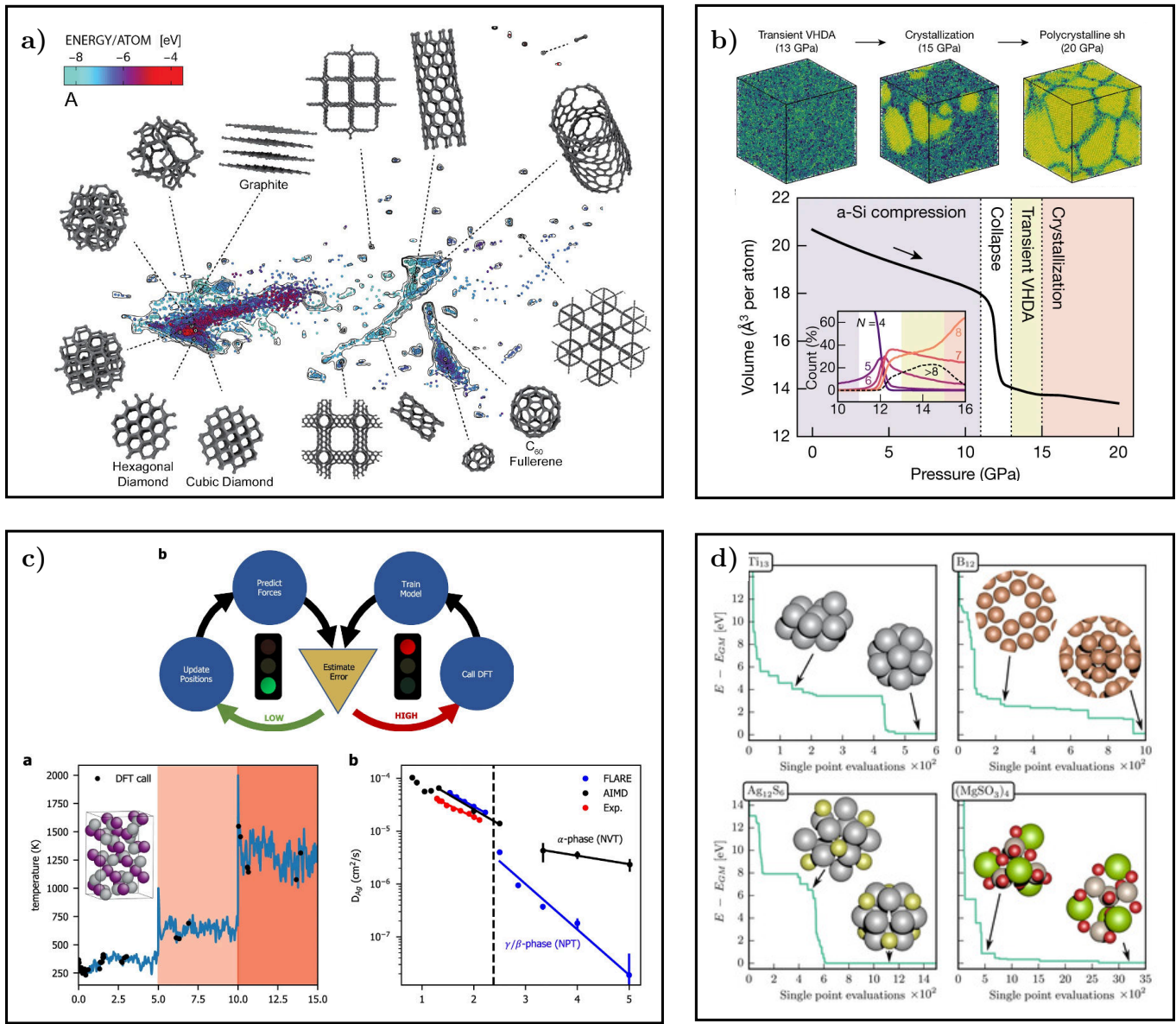


FIG. 7. Application of machine learning potentials using two different strategies. The top row highlights use cases as general-purpose potentials for elementary systems such as carbon (a)⁶² and silicon (b).¹¹⁴ The bottom row features examples of surrogate models for on-the-fly learning (c)¹⁴⁶ and global structure optimisation.¹⁴⁷

Another area of application of MLPs is in the modelling of complex aqueous systems, as summarised in the third set of examples in Fig. 8. The first one is on water flow in different nanotubes,¹⁵² where experiments have reported interesting radius and material dependence of the friction of water passing through. This study was able to fully resolve the radius dependence going to system sizes on the order of 10,000 atoms for multiple nanoseconds simulation time. Previous AIMD studies could only reach a few hundred picoseconds for system sizes on the order of 500 atoms. The second example shows the complex phase behaviour of a single layer of water under nanoconfinement.¹⁵³ This setup can be realised experimentally by sandwiching water in be-

tween graphene sheets. This work revealed a rich phase diagram as a function of temperature and pressure with two previously unreported phases for this system: A so-called hexatic phase, which is an intermediate between solid and liquid, and a superionic phase with very high propensity for proton transfer and thus high conductivity. In this case, the use of MLPs has enabled the study of this system at a level of complexity previously inaccessible by force fields and AIMD studies.

Finally, a big strength of MLPs over the traditional force field approaches is the ability to describe bond breaking and formation.^{44,45,156} Some of the examples above have already shown this, but the fourth set of examples in Fig. 8 highlights two studies that build more on

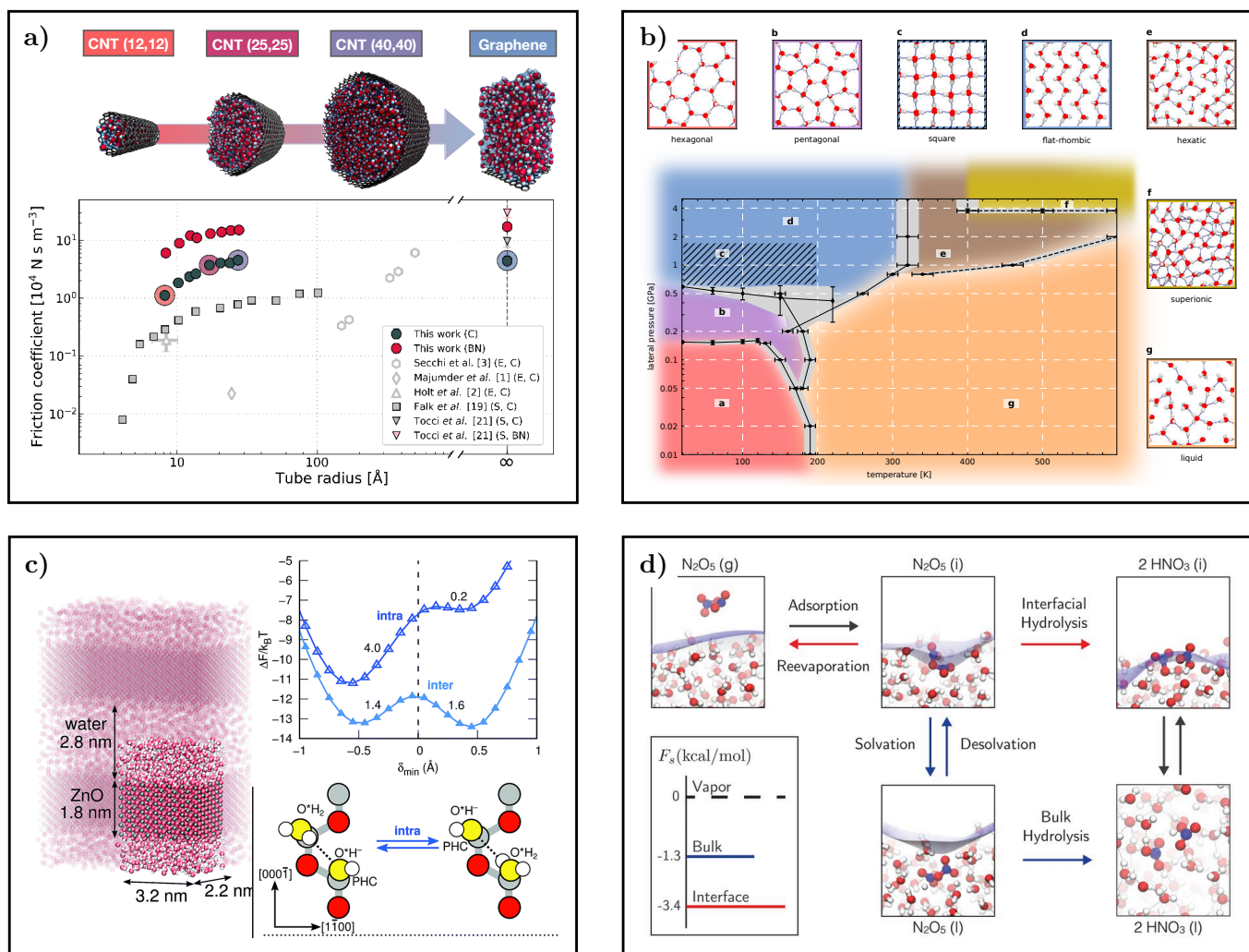


FIG. 8. Machine learning potentials applied to provide insight into complex aqueous systems. a) Water flow in nanotubes.¹⁵² b) Phase behaviour of nanoconfined monolayer water.¹⁵³ c) Water dissociation at a ZnO interface.¹⁵⁴ d) N_2O_5 decomposition at the water-air interface.¹⁵⁵

this capability. The first is on the dissociation of water at the ZnO interface,¹⁵⁴ relevant for catalytic processes. The second one shows the application of a neural network based model to understand the decomposition of N_2O_5 at the water-air interface,¹⁵⁵ relevant for climate science. Both of these studies provide insight into complex reactive processes at interfaces, which would be very difficult or impossible to describe using traditional approaches, thus clearly highlighting how machine learning pushes forward our ability to model complex processes with atomistic simulations.

Overall, these examples highlight the versatility of MLPs to provide insight into diverse areas of the natural sciences. The general-purpose models for carbon and silicon fall primarily into the category of material science, while the silver iodide application is an example of condensed matter physics. The applications to nanoconfined water showcase the ability of MLPs to study questions related to nanoscience. At the same time, the last two

on proton transfer reactions at interfaces belong to the field of acid-base chemistry, surface science, and catalysis. The selected examples are only a tiny fraction of the vibrant field, and many other applications to various other areas of the natural sciences are published daily. This use of a united set of tools over vastly different scientific areas is expected to continue. We foresee a great future for MLPs in providing atomistic insight across the fields.

VIII. SUMMARY AND OUTLOOK

The integration of machine learning into the representation of potential energy surfaces in atomistic simulations can greatly improve the accuracy and efficiency of these simulations. Traditional methods for representing PESs rely on fitting analytical functions to a limited set of data obtained from simulations or experiments. How-

ever, these methods can be limited in their ability to accurately represent the PESs for complex systems or materials. ML algorithms, on the other hand, can learn the underlying relationships between the atomic structure and the PES from a data-driven perspective, providing a more flexible and accurate representation of the PES. Furthermore, MLPs can also be used for larger systems than used in the training process, without the need for additional simulations. In some cases, even the application to previously unseen situations can be achieved, thus relying on the transferability of the model.^{62,157–159} However, this should only be done with great care, as extrapolation does, in general, not work with machine learning models. The first introduced methods HD-NNPs, GAP, and others have delivered great scientific insight and have paved the way for new developments which further transform the field of molecular and materials modelling.

Let us summarise the relevant concepts behind MLPs once more. First, a meaningful set of structures has to be curated, for example, with a force field or ab initio sampling in the initial stage. The coordinates of that initial training set are then transformed by a set of descriptors that incorporate the relevant invariances. Next, these are used as input for the regression model of choice, outputting atomic energy contributions for each atom in the system, summing up to the total potential energy. The model’s parameters are optimised by comparing the predicted energy (and usually the forces) to the reference values from the ab initio method of choice. Validation of important properties will show if this initial model is sufficient for the envisaged application. If not, the training set is expanded either by structure-based or property-based selection techniques (or both) and the process is repeated until a satisfactory quality is achieved. Once an initial model is available, new structures can readily be generated with that model, usually speeding up the exploration process. Meaningful error estimates can benefit this step as they enable the identification of outliers and validation of simulation results. Finally, the developed model passes all tests relevant to the application and can be applied to provide insight into challenging scientific questions.

The data-driven and automated approaches to develop new MLPs and select training data have significantly reduced the required number of reference calculations. This enables sophisticated electronic structure calculations to be used as a reference for the model, which would otherwise be too expensive for on-the-fly sampling. Examples include the use of converged coupled-cluster calculations for gas phase systems such as reactive protonated water clusters,^{160,161} organic molecules,¹⁶² and even models over chemical compound space.¹⁶³ Furthermore, it has been shown recently that these techniques can also be leveraged for condensed phase systems, as demonstrated for liquid water at coupled cluster accuracy,^{164,165} or high-pressure phases of hydrogen using variational Monte Carlo.¹⁶⁶ Some of these examples make use of techniques to further reduce the number of reference points, such as

delta learning,¹¹⁰ or transfer learning.^{163,167} The former represents only the difference between a high-level and a low-level method via machine learning, thus making the resulting delta-PES smoother and easier to learn. The latter uses a pre-trained model optimized to a large set of low-level reference points and retrains to a much smaller set of high-level points, thus transferring parts of the learned physics of the PES from the cheaper to the more demanding method. This push for high-quality reference methods is very promising and expected to flourish in the following years, opening up the possibility of describing yet more challenging systems at previously unattainable accuracy.

Another area where ML has the potential to improve and accelerate atomistic simulations is in the representation of other properties, such as dipole moments,^{125,168} or polarisabilities.¹⁶⁹ These properties are often difficult or expensive to calculate using traditional methods but can be equally well learned directly from reference data. They play a crucial role in determining the optical and electronic properties of materials, and their accurate prediction is essential for the rational design and optimisation of materials for technological applications. This also includes excited potential energy surfaces, enabling the treatment of electron excitation processes and excited state dynamics.^{42,170} Representing wave functions¹⁷¹ or electronic densities¹⁷² with ML is another active area of research, which has the potential to greatly improve the accuracy of quantum mechanical simulations. In these cases, rather than learning derived properties, the wave function is learned directly enabling all derived properties to be easily calculated.

One of the remaining challenges in representing PESs with ML is the long-range interactions between atoms.¹⁰ These interactions can have a significant impact on the properties of materials but require some degree of physics to be included in the ML model. Systems that are particularly impacted by short-sighted models include polar crystal surfaces,^{173,174} disordered interfaces such as the water-air interface,^{175,176} and systems with long-range charge transfer.⁷⁰ Recent work has shown that ML can be used to accurately represent these long-range interactions by using different techniques and this push towards more physics-inspired models is expected to continue.¹⁷⁷ These methods can accurately predict the PESs for a wide range of materials where long-range interactions are important, including disordered or polar interfaces.^{174,176,178}

Finally, the recent surge in the development of generalisable models, such as MACE-MP-0,¹¹⁵ MACE-OFF,¹¹⁶ GNoME,¹¹⁷ MatterSim,¹¹⁸ CHGNet,¹¹⁹ and others, highlights the potential for MLPs to deliver universal force fields applicable across chemical compound space. Their development and push towards more robustness and accuracy has only begun, but shows great promises even beyond the regimes set by their training data. Additional advantage of these models is in providing a starting point as structure generator and for fine

tuning according to specific needs of an application of interest in terms of chemical composition and electronic structure reference. Out of the many recent developments, this has led to exciting progress and will open up these tools to an even wider community, including non-expert users.

In conclusion, ML is revolutionising the way we represent and predict the properties of materials and reactions by atomistic simulations. The integration of ML into atomistic simulations has shown great promise in the representation of interatomic potential energy surfaces, prediction of other properties such as dipole moments, polarisabilities, and excited states. Representing wave functions or electronic densities with ML is also a promising area of research. There are still many open questions and challenges to be addressed, such as the long-range interactions, generalisation and interpretability. Nevertheless, machine learning for atomistic simulations has proven to be a game changer in the field, providing a new understanding of complex systems. It is here to stay and will continue to deliver exciting new approaches that make it possible to tackle more and more complex and challenging scientific problems.

ACKNOWLEDGMENTS

We would like to thank Gabor Csanyi, Jörg Behler, Ondrej Marsalek, and Dominik Marx for many discussions on this topic. C.S. acknowledges partial financial support from the *Alexander von Humboldt-Stiftung* and the Deutsche Forschungsgemeinschaft (DFG, German Research Foundation) project number 500244608. N.O.N acknowledges financial support from the Gates Cambridge Trust. V.K. acknowledges support from the Ernest Oppenheimer Early Career Fellowship and the Sydney Harvey Junior Research Fellowship, Churchill College, University of Cambridge. AM acknowledges support from the European Union under the “n-aqua” ERC project (101071937).

COMPETING INTERESTS

The authors declare no competing interests.

SUPPORTING INFORMATION

To better facilitate the understanding of the described concepts, we have developed a Colab online tutorial that walks users through all relevant steps of developing an MLP. It is focused on a simple, one component system, diamond, for which a training set is constructed using query by committee from a short reference simulation. Next, the resulting model is used for a longer simulation and validated with respect to the reference. This tutorial can be accessed via [Colab](#). An overview of

the most important ML concepts is provided in Tab.S1, while different open-source codes to develop machine learning potentials are compiled in Tab. S2 including links to the software packages as well as relevant citations.^{13–15,17,20,21,23,86–88,90,146,179–190}

- ¹J. Behler, “Perspective: Machine learning potentials for atomistic simulations,” *J. Chem. Phys.* **145**, 170901 (2016).
- ²J. Behler, “First Principles Neural Network Potentials for Reactive Simulations of Large Molecular and Condensed Systems,” *Angew. Chemie Int. Ed.* **56**, 12828–12840 (2017).
- ³A. P. Bartók, S. De, C. Poelking, N. Bernstein, J. R. Kermode, G. Csányi, and M. Ceriotti, “Machine learning unifies the modeling of materials and molecules,” *Sci. Adv.* **3**, e1701816 (2017).
- ⁴K. T. Butler, D. W. Davies, H. Cartwright, O. Isayev, and A. Walsh, “Machine learning for molecular and materials science,” *Nature* **559**, 547–555 (2018).
- ⁵V. L. Deringer, M. A. Caro, and G. Csányi, “Machine Learning Interatomic Potentials as Emerging Tools for Materials Science,” *Adv. Mater.* **31**, 1902765 (2019).
- ⁶P. L. Kang, C. Shang, and Z. P. Liu, “Large-Scale Atomic Simulation via Machine Learning Potentials Constructed by Global Potential Energy Surface Exploration,” *Acc. Chem. Res.* **53**, 2119–2129 (2020).
- ⁷F. Noé, A. Tkatchenko, K. R. Müller, and C. Clementi, “Machine Learning for Molecular Simulation,” *Annu. Rev. Phys. Chem.* **71**, 361–390 (2020).
- ⁸T. Mueller, A. Hernandez, and C. Wang, “Machine learning for interatomic potential models,” *J. Chem. Phys.* **152**, 50902 (2020).
- ⁹M. Ceriotti, C. Clementi, and O. A. von Lilienfeld, “Machine learning meets chemical physics,” *J. Chem. Phys.* **154**, 160401 (2021).
- ¹⁰J. Behler and G. Csányi, “Machine learning potentials for extended systems: a perspective,” *Eur. Phys. J. B* **94**, 1–11 (2021).
- ¹¹O. T. Unke, S. Chmiela, H. E. Sauceda, M. Gastegger, I. Poltavsky, K. T. Schütt, A. Tkatchenko, and K. R. Müller, “Machine Learning Force Fields,” *Chem. Rev.* **121**, 10142–10186 (2021).
- ¹²E. Kocer, T. W. Ko, and J. Behler, “Neural Network Potentials: A Concise Overview of Methods,” *Annu. Rev. Phys. Chem.* **73**, 163–186 (2022).
- ¹³J. Behler and M. Parrinello, “Generalized Neural-Network Representation of High-Dimensional Potential-Energy Surfaces,” *Phys. Rev. Lett.* **98**, 146401 (2007).
- ¹⁴A. P. Bartók, M. C. Payne, R. Kondor, and G. Csányi, “Gaussian approximation potentials: The accuracy of quantum mechanics, without the electrons,” *Phys. Rev. Lett.* **104**, 1902765 (2010).
- ¹⁵A. V. Shapeev, “Moment tensor potentials: A class of systematically improvable interatomic potentials,” *Multiscale Model. Simul.* **14**, 1153–1173 (2016).
- ¹⁶I. S. Novikov, K. Gubaev, E. V. Podryabinkin, and A. V. Shapeev, “The MLIP package: moment tensor potentials with MPI and active learning,” *Mach. Learn. Sci. Technol.* **2**, 25002 (2020).
- ¹⁷R. Drautz, “Atomic cluster expansion for accurate and transferable interatomic potentials,” *Phys. Rev. B* **99**, 014104 (2019).
- ¹⁸A. P. Thompson, L. P. Swiler, C. R. Trott, S. M. Foiles, and G. J. Tucker, “Spectral neighbor analysis method for automated generation of quantum-accurate interatomic potentials,” *J. Comput. Phys.* **285**, 316–330 (2015).
- ¹⁹M. A. Wood and A. P. Thompson, “Extending the accuracy of the SNAP interatomic potential form,” *J. Chem. Phys.* **148**, 241721 (2018).
- ²⁰I. Batatia, D. P. Kovács, G. N. C. Simm, C. Ortner, and G. Csányi, “MACE: Higher Order Equivariant Message Passing Neural Networks for Fast and Accurate Force Fields,” *Adv. Neural Inf. Process. Syst.* **35**, 11423–11436 (2022).

- ²¹O. T. Unke and M. Meuwly, “PhysNet: A Neural Network for Predicting Energies, Forces, Dipole Moments, and Partial Charges,” *J. Chem. Theory Comput.* **15**, 3678–3693 (2019).
- ²²R. Zubatyuk, J. S. Smith, J. Leszczynski, and O. Isayev, “Accurate and transferable multitask prediction of chemical properties with an atoms-in-molecules neural network,” *Sci. Adv.* **5**, eaav6490 (2019).
- ²³S. Batzner, A. Musaelian, L. Sun, M. Geiger, J. P. Mailoa, M. Kornbluth, N. Molinari, T. E. Smidt, and B. Kozinsky, “E(3)-Equivariant Graph Neural Networks for Data-Efficient and Accurate Interatomic Potentials,” *Nat. Commun.* **13**, 1–11 (2021).
- ²⁴K. T. Schütt, O. T. Unke, and M. Gastegger, “Equivariant message passing for the prediction of tensorial properties and molecular spectra,” *Proc. 38th Int. Conf. Mach. Learn.* **139**, 9377–9388 (2021).
- ²⁵L. Zhang, J. Han, H. Wang, R. Car, and E. Weinan, “Deep Potential Molecular Dynamics: A Scalable Model with the Accuracy of Quantum Mechanics,” *Phys. Rev. Lett.* **120**, 143001 (2018).
- ²⁶H. Wang, L. Zhang, J. Han, and W. E, “DeePMD-kit: A deep learning package for many-body potential energy representation and molecular dynamics,” *Comput. Phys. Commun.* **228**, 178–184 (2018).
- ²⁷K. T. Schütt, H. E. Sauceda, P. J. Kindermans, A. Tkatchenko, and K. R. Müller, “SchNet - A deep learning architecture for molecules and materials,” *J. Chem. Phys.* **148**, 241722 (2018).
- ²⁸A. Singraber, J. Behler, and C. Dellago, “Library-Based LAMMPS Implementation of High-Dimensional Neural Network Potentials,” *J. Chem. Theory Comput.* **15**, 1827–1840 (2019).
- ²⁹M. S. Chen, T. Morawietz, H. Mori, T. E. Markland, and N. Artrith, “AENET-LAMMPS and AENET-TINKER: Interfaces for accurate and efficient molecular dynamics simulations with machine learning potentials,” *J. Chem. Phys.* **155**, 74801 (2021).
- ³⁰D. Lu, H. Wang, M. Chen, L. Lin, R. Car, W. E, W. Jia, and L. Zhang, “86 PFLOPS Deep Potential Molecular Dynamics simulation of 100 million atoms with ab initio accuracy,” *Comput. Phys. Commun.* **259**, 107624 (2021).
- ³¹A. Musaelian, S. Batzner, A. Johansson, L. Sun, C. J. Owen, M. Kornbluth, and B. Kozinsky, “Learning local equivariant representations for large-scale atomistic dynamics,” *Nat. Commun.* **14**, 579 (2023).
- ³²J. Behler, “Neural network potential-energy surfaces in chemistry: a tool for large-scale simulations,” *Phys. Chem. Chem. Phys.* **13**, 17930–17955 (2011).
- ³³J. Behler, “Representing potential energy surfaces by high-dimensional neural network potentials,” *J. Phys. Condens. Matter* **26**, 183001 (2014).
- ³⁴J. Behler, “Constructing high-dimensional neural network potentials: A tutorial review,” *Int. J. Quantum Chem.* **115**, 1032–1050 (2015).
- ³⁵J. Behler, “Four Generations of High-Dimensional Neural Network Potentials,” *Chem. Rev.* **121**, 10037–10072 (2021).
- ³⁶A. P. Bartók and G. Csányi, “Gaussian approximation potentials: A brief tutorial introduction,” *Int. J. Quantum Chem.* **115**, 1051–1057 (2015).
- ³⁷V. L. Deringer, A. P. Bartók, N. Bernstein, D. M. Wilkins, M. Ceriotti, and G. Csányi, “Gaussian Process Regression for Materials and Molecules,” *Chem. Rev.* **121**, 10073–10141 (2021).
- ³⁸G. R. Schleder, A. C. Padilha, C. M. Acosta, M. Costa, and A. Fazzio, “From DFT to machine learning: recent approaches to materials science—a review,” *J. Phys. Mater.* **2**, 032001 (2019).
- ³⁹Y. Mishin, “Machine-learning interatomic potentials for materials science,” *Acta Mater.* **214**, 116980 (2021).
- ⁴⁰T. Zubatyuk and O. Isayev, “Development of Multimodal Machine Learning Potentials: Toward a Physics-Aware Artificial Intelligence,” *Acc. Chem. Res.* **54**, 1575–1585 (2021).
- ⁴¹F. Musil, A. Grisafi, A. P. Bartók, C. Ortner, G. Csányi, and M. Ceriotti, “Physics-Inspired Structural Representations for Molecules and Materials,” *Chem. Rev.* **121**, 9759–9815 (2021).
- ⁴²J. Westermayr and P. Marquetand, “Machine Learning for Electronically Excited States of Molecules,” *Chem. Rev.* **121**, 9873–9926 (2021).
- ⁴³B. Huang and O. A. Von Lilienfeld, “Ab Initio Machine Learning in Chemical Compound Space,” *Chem. Rev.* **121**, 10001–10036 (2021).
- ⁴⁴S. Manzhos and T. Carrington, “Neural Network Potential Energy Surfaces for Small Molecules and Reactions,” *Chem. Rev.* **121**, 10187–10217 (2021).
- ⁴⁵M. Meuwly, “Machine Learning for Chemical Reactions,” *Chem. Rev.* **121**, 10218–10239 (2021).
- ⁴⁶D. M. Anstine and O. Isayev, “Machine Learning Interatomic Potentials and Long-Range Physics,” *J. Phys. Chem. A* **127**, 2417–2431 (2022).
- ⁴⁷A. M. Miksch, T. Morawietz, J. Kästner, A. Urban, and N. Artrith, “Strategies for the construction of machine-learning potentials for accurate and efficient atomic-scale simulations,” *Mach. Learn. Sci. Technol.* **2**, 031001 (2021).
- ⁴⁸M. F. Langer, A. Goeßmann, and M. Rupp, “Representations of molecules and materials for interpolation of quantum-mechanical simulations via machine learning,” *npj Comput. Mater.* **8**, 1–14 (2022).
- ⁴⁹A. Zheng, K. Liang, L. Zhang, al, A. Goscinski, G. Fraux, G. Imbalzano, and M. Ceriotti, “The role of feature space in atomistic learning,” *Mach. Learn. Sci. Technol.* **2**, 25028 (2021).
- ⁵⁰M. Rupp, A. Tkatchenko, K. R. Müller, and O. A. Von Lilienfeld, “Fast and accurate modeling of molecular atomization energies with machine learning,” *Phys. Rev. Lett.* **108**, 058301 (2012).
- ⁵¹T. B. Blank, S. D. Brown, A. W. Calhoun, and D. J. Doren, “Neural network models of potential energy surfaces,” *J. Chem. Phys.* **103**, 4129 (1998).
- ⁵²D. F. R. Brown, M. N. Gibbs, and D. C. Clary, “Combining ab initio computations, neural networks, and diffusion Monte Carlo: An efficient method to treat weakly bound molecules,” *J. Chem. Phys.* **105**, 7597 (1998).
- ⁵³S. Lorenz, A. Groß, and M. Scheffler, “Representing high-dimensional potential-energy surfaces for reactions at surfaces by neural networks,” *Chem. Phys. Lett.* **395**, 210–215 (2004).
- ⁵⁴J. Behler, “Atom-centered symmetry functions for constructing high-dimensional neural network potentials,” *J. Chem. Phys.* **134**, 074106 (2011).
- ⁵⁵K. V. Jose, N. Artrith, and J. Behler, “Construction of high-dimensional neural network potentials using environment-dependent atom pairs,” *J. Chem. Phys.* **136**, 194111 (2012).
- ⁵⁶M. Gastegger, L. Schwiedrzik, M. Bittermann, F. Berzsenyi, and P. Marquetand, “wACSF—Weighted atom-centered symmetry functions as descriptors in machine learning potentials,” *J. Chem. Phys.* **148**, 241709 (2018).
- ⁵⁷M. P. Bircher, A. Singraber, and C. Dellago, “Improved description of atomic environments using low-cost polynomial functions with compact support,” *Mach. Learn. Sci. Technol.* **2**, 35026 (2021).
- ⁵⁸A. P. Bartók, R. Kondor, and G. Csányi, “On representing chemical environments,” *Phys. Rev. B* **87**, 184115 (2013).
- ⁵⁹W. J. Szlachta, A. P. Bartók, and G. Csányi, “Accuracy and transferability of GAP models for tungsten,” *Phys. Rev. B* **90**, 104108 (2014).
- ⁶⁰P. Rowe, G. Csányi, D. Alfè, and A. Michaelides, “Development of a machine learning potential for graphene,” *Phys. Rev. B* **97**, 54303 (2018).
- ⁶¹F. L. Thiemann, P. Rowe, E. A. Müller, and A. Michaelides, “Machine Learning Potential for Hexagonal Boron Nitride Applied to Thermally and Mechanically Induced Rippling,” *J. Phys. Chem. C* **124**, 22278–22290 (2020).
- ⁶²P. Rowe, V. L. Deringer, P. Gasparotto, G. Csányi, and A. Michaelides, “An accurate and transferable machine learn-

- ing potential for carbon,” *J. Chem. Phys.* **153**, 034702 (2020).
- ⁶³P. Rowe, V. L. Deringer, P. Gasparotto, G. Csányi, and A. Michaelides, “Erratum: An accurate and transferable machine learning potential for carbon (J. Chem. Phys. (2020) 153 (034702) DOI: 10.1063/5.0005084),” *J. Chem. Phys.* **156**, 159901 (2022).
- ⁶⁴G. Imbalzano, A. Anelli, D. Giofré, S. Klees, J. Behler, and M. Ceriotti, “Automatic selection of atomic fingerprints and reference configurations for machine-learning potentials,” *J. Chem. Phys.* **148**, 241730 (2018).
- ⁶⁵M. A. Caro, “Optimizing many-body atomic descriptors for enhanced computational performance of machine learning based interatomic potentials,” *Phys. Rev. B* **100**, 24112 (2019).
- ⁶⁶J. P. Darby, D. P. Kovács, I. Batatia, M. A. Caro, G. L. W. Hart, C. Ortner, and G. Csányi, “Tensor-reduced atomic density representations,” *arXiv* (2022), 10.48550/arxiv.2210.01705.
- ⁶⁷S. N. Pozdnyakov, M. J. Willatt, A. P. Bartók, C. Ortner, G. Csányi, and M. Ceriotti, “Incompleteness of Atomic Structure Representations,” *Phys. Rev. Lett.* **125**, 166001 (2020).
- ⁶⁸A. V. Shapeev, “Moment Tensor Potentials: a class of systematically improvable interatomic potentials,” *Multiscale Model. Simul.* **14**, 1153–1173 (2015).
- ⁶⁹N. Artrith, T. Morawietz, and J. Behler, “High-dimensional neural-network potentials for multicomponent systems: Applications to zinc oxide,” *Phys. Rev. B - Condens. Matter Mater. Phys.* **83**, 153101 (2011).
- ⁷⁰T. W. Ko, J. A. Finkler, S. Goedecker, and J. Behler, “A fourth-generation high-dimensional neural network potential with accurate electrostatics including non-local charge transfer,” *Nat. Commun.* **12**, 1–11 (2021).
- ⁷¹A. Grisafi and M. Ceriotti, “Incorporating long-range physics in atomic-scale machine learning,” *J. Chem. Phys.* **151**, 204105 (2019).
- ⁷²J. Gilmer, S. S. Schoenholz, P. F. Riley, O. Vinyals, and G. E. Dahl, “Neural Message Passing for Quantum Chemistry,” *ICML’17 Proc. 34th Int. Conf. Mach. Learn.* **70**, 1263–1272 (2017).
- ⁷³S. O. Haykin, *Neural Networks and Learning Machines*, 3rd ed. (Pearson, New York, 2008).
- ⁷⁴T. B. Blank and S. D. Brown, “Adaptive, global, extended Kalman filters for training feedforward neural networks,” *J. Chemom.* **8**, 391–407 (1994).
- ⁷⁵J. B. Witkoskie and D. J. Doren, “Neural Network Models of Potential Energy Surfaces: Prototypical Examples,” *J. Chem. Theory Comput.* **1**, 14–23 (2005).
- ⁷⁶M. Gastegger and P. Marquetand, “Molecular Dynamics with Neural Network Potentials,” *Lect. Notes Phys.* **968**, 233–252 (2020).
- ⁷⁷N. Bernstein, B. Bhattarai, G. Csányi, D. A. Drabold, S. R. Elliott, V. L. Deringer, N. Bernstein, B. Bhattarai, R. D. A. Drabold, G. Csányi, V. L. Deringer, and S. R. Elliott, “Quantifying Chemical Structure and Machine-Learned Atomic Energies in Amorphous and Liquid Silicon,” *Angew. Chemie Int. Ed.* **58**, 7057–7061 (2019).
- ⁷⁸S. Chong, F. Grasselli, C. B. Mahmoud, J. D. Morrow, V. L. Deringer, and M. Ceriotti, “Robustness of Local Predictions in Atomistic Machine Learning Models,” *arXiv* (2023).
- ⁷⁹D. M. Hawkins, “The Problem of Overfitting,” *J. Chem. Inf. Comput. Sci.* **44**, 1–12 (2004).
- ⁸⁰S. Shah, F. Palmieri, and M. Datum, “Optimal filtering algorithms for fast learning in feedforward neural networks,” *Neural Networks* **5**, 779–787 (1992).
- ⁸¹C. E. Rasmussen and C. K. I. Williams, *Gaussian Process. Mach. Learn.* (The MIT Press, 2018).
- ⁸²V. L. Deringer and G. Csányi, “Machine learning based interatomic potential for amorphous carbon,” *Phys. Rev. B* **95**, 94203 (2017).
- ⁸³C. Schran, K. Brezina, and O. Marsalek, “Committee neural network potentials control generalization errors and enable active learning,” *J. Chem. Phys.* **153**, 104105 (2020).
- ⁸⁴T. W. Ko, J. A. Finkler, S. Goedecker, and J. Behler, “General-Purpose Machine Learning Potentials Capturing Non-local Charge Transfer,” *Acc. Chem. Res.* **54**, 808–817 (2021).
- ⁸⁵R. Zubatyuk, J. S. Smith, B. T. Nebgen, S. Tretiak, and O. Isayev, “Teaching a neural network to attach and detach electrons from molecules,” *Nat. Commun.* **12**, 1–11 (2021).
- ⁸⁶A. Bochkarev, Y. Lysogorskiy, S. Menon, M. Qamar, M. Mrovec, and R. Drautz, “Efficient parametrization of the atomic cluster expansion,” *Phys. Rev. Mater.* **6**, 013804 (2022).
- ⁸⁷Z. Fan, Y. Wang, P. Ying, K. Song, J. Wang, Y. Wang, Z. Zeng, K. Xu, E. Lindgren, J. M. Rahm, A. J. Gabourie, J. Liu, H. Dong, J. Wu, Y. Chen, Z. Zhong, J. Sun, P. Erhart, Y. Su, and T. Ala-Nissila, “GPUMD: A package for constructing accurate machine-learned potentials and performing highly efficient atomistic simulations,” *J. Chem. Phys.* **157**, 114801 (2022).
- ⁸⁸Y. Lysogorskiy, C. van der Oord, A. Bochkarev, S. Menon, M. Rinaldi, T. Hammerschmidt, M. Mrovec, A. Thompson, G. Csányi, C. Ortner, and R. Drautz, “Performant implementation of the atomic cluster expansion (PACE) and application to copper and silicon,” *npj Comput. Mater.* **7**, 1–12 (2021).
- ⁸⁹D. P. Kovács, C. V. D. Oord, J. Kucera, A. E. Allen, D. J. Cole, C. Ortner, and G. Csányi, “Linear Atomic Cluster Expansion Force Fields for Organic Molecules: Beyond RMSE,” *J. Chem. Theory Comput.* **17**, 7696–7711 (2021).
- ⁹⁰I. Batatia, S. Batzner, D. P. Kovács, A. Musaelian, G. N. C. Simm, R. Drautz, C. Ortner, B. Kozinsky, and G. Csányi, “The Design Space of E(3)-Equivariant Atom-Centered Interatomic Potentials,” *arXiv* (2022), 10.48550/arxiv.2205.06643.
- ⁹¹J. Gastegger, J. Groß, and S. Günnemann, “Directional Message Passing for Molecular Graphs,” in *8th Int. Conf. Learn. Represent. ICLR 2020* (International Conference on Learning Representations, ICLR, 2020) *arXiv:2003.03123*.
- ⁹²K. T. Schütt, O. T. Unke, and M. Gastegger, “Equivariant message passing for the prediction of tensorial properties and molecular spectra,” in *Proc. Mach. Learn. Res.*, Vol. 139 (ML Research Press, 2021) pp. 9377–9388, *arXiv:2102.03150*.
- ⁹³Mojtaba Haghghatlari, Jie Li, Xingyi Guan, Oufan Zhang, Akshaya Das, C. J. Stein, Farnaz Heidar-Zadeh, Meili Liu, Martin Head-Gordon, Luke Bertels, Hongxia Hao, Itai Leven, and Teresa Head-Gordon, “NewtonNet: a Newtonian message passing network for deep learning of interatomic potentials and forces,” *Digit. Discov.* **1**, 333–343 (2022).
- ⁹⁴J. Brandstetter, R. Hesselink, E. van der Pol, E. J. Bekkers, and M. Welling, “Geometric and Physical Quantities Improve E(3) Equivariant Message Passing,” in *Int. Conf. Learn. Represent.* (International Conference on Learning Representations, ICLR, 2022) *arXiv:2110.02905*.
- ⁹⁵F. B. Fuchs, D. E. Worrall, V. Fischer, and M. Welling, “SE(3)-transformers: 3D roto-translation equivariant attention networks,” in *Adv. Neural Inf. Process. Syst.* (2020) pp. 1970–1981, *arXiv:2006.10503*.
- ⁹⁶Y.-L. Liao and T. Smidt, “Equiformer: Equivariant Graph Attention Transformer for 3D Atomistic Graphs,” in *Int. Conf. Learn. Represent.* (2023) *arXiv:arXiv:2206.11990*.
- ⁹⁷P. Thölke and G. De Fabritiis, “TorchMD-NET: Equivariant Transformers for Neural Network based Molecular Potentials,” in *Int. Conf. Learn. Represent.* (International Conference on Learning Representations, ICLR, 2022) *arXiv:2202.02541*.
- ⁹⁸S. Passaro and C. L. Zitnick, “Reducing SO(3) Convolutions to SO(2) for Efficient Equivariant GNNs,” in *Int. Conf. Mach. Learn.* (PMLR, 2023) pp. 27420–27438, *arXiv:2302.03655*.
- ⁹⁹A. Musaelian, S. Batzner, A. Johansson, L. Sun, C. J. Owen, M. Kornbluth, and B. Kozinsky, “Learning local equivariant representations for large-scale atomistic dynamics,” *Nat. Commun.* **2023 141 14**, 1–15 (2023).
- ¹⁰⁰I. Batatia, S. Batzner, D. P. Kovács, A. Musaelian, G. N. C. Simm, R. Drautz, C. Ortner, B. Kozinsky, and G. Csányi, “The Design Space of E(3)-Equivariant Atom-Centered Interatomic Potentials,” *arXiv* (2022).

- ¹⁰¹A. Bochkarev, Y. Lysogorskiy, C. Ortner, G. Csányi, and R. Drautz, "Multilayer atomic cluster expansion for semilocal interactions," *Phys. Rev. Res.* **4**, L042019 (2022).
- ¹⁰²J. Nigam, S. Pozdnyakov, G. Fraux, and M. Ceriotti, "Unified theory of atom-centered representations and message-passing machine-learning schemes," *J. Chem. Phys.* **156**, 204115 (2022).
- ¹⁰³D. P. Kovacs, I. Batatia, E. S. Arany, and G. Csányi, "Evaluation of the MACE Force Field Architecture: from Medicinal Chemistry to Materials Science," *J. Chem. Phys.* **159**, 44118 (2023).
- ¹⁰⁴C. Chen and S. P. Ong, "A universal graph deep learning interatomic potential for the periodic table," *Nat. Comput. Sci.* **2**, 718–728 (2022).
- ¹⁰⁵S. Yue, M. C. Muniz, M. F. Andrade, L. Zhang, R. Car, and A. Z. Panagiotopoulos, "When do short-range atomistic machine-learning models fall short?" *J. Chem. Phys.* **154**, 34111 (2021).
- ¹⁰⁶K. Yao, J. E. Herr, D. W. Toth, R. McKintyre, and J. Parkhill, "The TensorMol-0.1 model chemistry: a neural network augmented with long-range physics," *Chem. Sci.* **9**, 2261–2269 (2018).
- ¹⁰⁷S. Grimme, "Semiempirical GGA-type density functional constructed with a long-range dispersion correction," *J. Comput. Chem.* **27**, 1787–1799 (2006).
- ¹⁰⁸Z. Deng, C. Chen, X. G. Li, and S. P. Ong, "An electrostatic spectral neighbor analysis potential for lithium nitride," *npj Comput. Mater.* **2019** **5**, 1–8 (2019).
- ¹⁰⁹P. Bleiziffer, K. Schaller, and S. Riniker, "Machine Learning of Partial Charges Derived from High-Quality Quantum-Mechanical Calculations," *J. Chem. Inf. Model.* **58**, 579–590 (2018).
- ¹¹⁰R. Ramakrishnan, P. O. Dral, M. Rupp, and O. A. Von Lilienfeld, "Big data meets quantum chemistry approximations: The Δ -machine learning approach," *J. Chem. Theory Comput.* **11**, 2087–2096 (2015).
- ¹¹¹B. Nebgen, N. Lubbers, J. S. Smith, A. E. Sifain, A. Lokhov, O. Isayev, A. E. Roitberg, K. Barros, and S. Tretiak, "Transferable Dynamic Molecular Charge Assignment Using Deep Neural Networks," *J. Chem. Theory Comput.* **14**, 4687–4698 (2018).
- ¹¹²D. P. Metcalf, A. Jiang, S. A. Spronk, D. L. Cheney, and C. D. Sherrill, "Electron-Passing Neural Networks for Atomic Charge Prediction in Systems with Arbitrary Molecular Charge," *J. Chem. Inf. Model.* **61**, 115–122 (2021).
- ¹¹³S. Chmiela, V. Vassilev-Galindo, O. T. Unke, A. Kabylda, H. E. Sauceda, A. Tkatchenko, and K. R. Müller, "Accurate global machine learning force fields for molecules with hundreds of atoms," *Sci. Adv.* **9** (2023), 10.1126/SCIADV.ADF0873.
- ¹¹⁴V. L. Deringer, N. Bernstein, G. Csányi, C. Ben Mahmoud, M. Ceriotti, M. Wilson, D. A. Drabold, and S. R. Elliott, "Origins of structural and electronic transitions in disordered silicon," *Nature* **589**, 59–64 (2021).
- ¹¹⁵I. Batatia, P. Benner, Y. Chiang, A. M. Elena, D. P. Kovács, J. Riebesell, X. R. Advincula, M. Asta, W. J. Baldwin, N. Bernstein, A. Bhowmik, S. M. Blau, V. Cărare, J. P. Darby, S. De, F. D. Pia, V. L. Deringer, R. Elijošius, Z. El-Machachi, E. Fako, A. C. Ferrari, A. Genreith-Schriever, J. George, R. E. A. Goodall, C. P. Grey, S. Han, W. Handley, H. H. Heenen, K. Hermansson, C. Holm, J. Jaafar, S. Hofmann, K. S. Jakob, H. Jung, V. Kapil, A. D. Kaplan, N. Karimitari, N. Kroupa, J. Kullgren, M. C. Kuner, D. Kuryla, G. Liepuoniute, J. T. Margraf, I.-B. Magdău, A. Michaelides, J. H. Moore, A. A. Naik, S. P. Niblett, S. W. Norwood, N. O'Neill, C. Ortner, K. A. Persson, K. Reuter, A. S. Rosen, L. L. Schaaf, C. Schran, E. Sivonxay, T. K. Stenczel, V. Svahn, C. Sutton, C. van der Oord, E. Varga-Umbrich, T. Vegge, M. Vondrák, Y. Wang, W. C. Witt, F. Zills, and G. Csányi, "A foundation model for atomistic materials chemistry," (2023), [arXiv:2401.00096](https://arxiv.org/abs/2401.00096) [physics.chem-ph].
- ¹¹⁶D. P. Kovács, J. H. Moore, N. J. Browning, I. Batatia, J. T. Horton, V. Kapil, W. C. Witt, I.-B. Magdău, D. J. Cole, and G. Csányi, "Mace-off23: Transferable machine learning force fields for organic molecules," (2023), [arXiv:2312.15211](https://arxiv.org/abs/2312.15211).
- ¹¹⁷A. Merchant, S. Batzner, S. S. Schoenholz, M. Aykol, G. Cheon, and E. D. Cubuk, "Scaling deep learning for materials discovery," *Nature* **624**, 80–85 (2023).
- ¹¹⁸H. Yang, C. Hu, Y. Zhou, X. Liu, Y. Shi, J. Li, G. Li, Z. Chen, S. Chen, C. Zeni, M. Horton, R. Pinsler, A. Fowler, D. Zügner, T. Xie, J. Smith, L. Sun, Q. Wang, L. Kong, C. Liu, H. Hao, and Z. Lu, "Mattersim: A deep learning atomistic model across elements, temperatures and pressures," (2024), [arXiv:2405.04967](https://arxiv.org/abs/2405.04967) [cond-mat.mtrl-sci].
- ¹¹⁹B. Deng, P. Zhong, K. Jun, J. Riebesell, K. Han, C. J. Bartel, and G. Ceder, "Chgnet: Pretrained universal neural network potential for charge-informed atomistic modeling," (2023), [arXiv:2302.14231](https://arxiv.org/abs/2302.14231) [cond-mat.mtrl-sci].
- ¹²⁰S. De, A. P. Bartók, G. Csányi, and M. Ceriotti, "Comparing molecules and solids across structural and alchemical space," *Phys. Chem. Chem. Phys.* **18**, 13754–13769 (2016).
- ¹²¹M. O. J. Jäger, E. V. Morooka, F. F. Canova, L. Himanen, and A. S. Foster, "Machine learning hydrogen adsorption on nanoclusters through structural descriptors," *npj Comput. Mater.* **4**, 1–8 (2018).
- ¹²²J. S. Smith, O. Isayev, and A. E. Roitberg, "ANI-1: an extensible neural network potential with DFT accuracy at force field computational cost," *Chem. Sci.* **8**, 3192–3203 (2017).
- ¹²³K. Brezina, H. Beck, and O. Marsalek, "Reducing the cost of neural network potential generation for reactive molecular systems," [arXiv \(2023\)](https://arxiv.org/abs/2023.10.48550), 10.48550/arXiv.2303.15521.
- ¹²⁴K. Gubaev, E. V. Podryabinkin, and A. V. Shapeev, "Machine learning of molecular properties: Locality and active learning," *J. Chem. Phys.* **148**, 241727 (2018).
- ¹²⁵M. Gastegger, J. Behler, and P. Marquetand, "Machine learning molecular dynamics for the simulation of infrared spectra," *Chem. Sci.* **8**, 6924–6935 (2017).
- ¹²⁶E. V. Podryabinkin and A. V. Shapeev, "Active learning of linearly parametrized interatomic potentials," *Comput. Mater. Sci.* **140**, 171–180 (2017).
- ¹²⁷J. S. Smith, B. Nebgen, N. Lubbers, O. Isayev, and A. E. Roitberg, "Less is more: Sampling chemical space with active learning," *J. Chem. Phys.* **148**, 241733 (2018).
- ¹²⁸V. L. Deringer, C. J. Pickard, and G. Csányi, "Data-Driven Learning of Total and Local Energies in Elemental Boron," *Phys. Rev. Lett.* **120**, 156001 (2018).
- ¹²⁹L. Zhang, D. Y. Lin, H. Wang, R. Car, and E. Weinan, "Active learning of uniformly accurate interatomic potentials for materials simulation," *Phys. Rev. Mater.* **3**, 023804 (2019).
- ¹³⁰F. Musil, M. J. Willatt, M. A. Langovoy, and M. Ceriotti, "Fast and Accurate Uncertainty Estimation in Chemical Machine Learning," *J. Chem. Theory Comput.* **15**, 906–915 (2019).
- ¹³¹Y. Zhai, A. Caruso, S. Gao, and F. Paesani, "Active learning of many-body configuration space: Application to the Cs+–water MB-nrg potential energy function as a case study," *J. Chem. Phys.* **152**, 144103 (2020).
- ¹³²R. Jinnouchi, F. Karsai, C. Verdi, R. Asahi, and G. Kresse, "Descriptors representing two- and three-body atomic distributions and their effects on the accuracy of machine-learned interatomic potentials," *J. Chem. Phys.* **152**, 234102 (2020).
- ¹³³Q. Lin, Y. Zhang, B. Zhao, and B. Jiang, "Automatically growing global reactive neural network potential energy surfaces: A trajectory-free active learning strategy," *J. Chem. Phys.* **152**, 154104 (2020).
- ¹³⁴J. P. Janet, C. Duan, T. Yang, A. Nandy, and H. J. Kulik, "A quantitative uncertainty metric controls error in neural network-driven chemical discovery," *Chem. Sci.* **10**, 7913–7922 (2019).
- ¹³⁵J. Carrete, H. Montes-Campos, R. Wanzelböck, E. Heid, and G. K. H. Madsen, "Deep Ensembles vs. Committees for Uncertainty Estimation in Neural-Network Force Fields: Comparison and Application to Active Learning," *J. Chem. Phys.* **158**, 204801 (2023).
- ¹³⁶G. Imbalzano, Y. Zhuang, V. Kapil, K. Rossi, E. A. Engel, F. Grasselli, and M. Ceriotti, "Uncertainty estimation for molec-

- ular dynamics and sampling,” *J. Chem. Phys.* **154**, 074102 (2021).
- ¹³⁷A. Krogh and J. Vedelsby, “Neural Network Ensembles, Cross Validation, and Active Learning,” *Adv. Neural Inf. Process. Syst.* **7** (1994).
- ¹³⁸H. S. Seung, M. Opper, and H. Sompolinsky, “Query by committee,” (Association for Computing Machinery, 1992) pp. 287–294.
- ¹³⁹C. van der Oord, M. Sachs, D. P. Kovács, C. Ortner, and G. Csányi, “Hyperactive Learning (HAL) for Data-Driven Interatomic Potentials,” *arXiv* (2022), 10.48550/arXiv.2210.04225.
- ¹⁴⁰M. Kulichenko, K. Barros, N. Lubbers, Y. W. Li, R. Messerly, S. Tretiak, J. S. Smith, and B. Nebgen, “Uncertainty-driven dynamics for active learning of interatomic potentials,” *Nat. Comput. Sci.* **3**, 230–239 (2023).
- ¹⁴¹J. D. Morrow, J. L. A. Gardner, and V. L. Deringer, “How to validate machine-learned interatomic potentials,” *J. Chem. Phys.* **158**, 121501 (2023).
- ¹⁴²D. Frenkel and B. Smit, *Underst. Mol. Simul.*, 2nd ed. (Academic Press, Inc., 2001).
- ¹⁴³M. Pinheiro, F. Ge, N. Ferré, P. O. Dral, and M. Barbatti, “Choosing the right molecular machine learning potential,” *Chem. Sci.* **12**, 14396–14413 (2021).
- ¹⁴⁴C. Schran, F. L. Thiemann, P. Rowe, E. A. Müller, O. Marsalek, and A. Michaelides, “Machine learning potentials for complex aqueous systems made simple,” *Proc. Natl. Acad. Sci.* **118**, e2110077118 (2021).
- ¹⁴⁵F. L. Thiemann, P. Rowe, A. Zen, E. A. Müller, and A. Michaelides, “Defect-Dependent Corrugation in Graphene,” *Nano Lett.* **21**, 8143–8150 (2021).
- ¹⁴⁶J. Vandermause, S. B. Torrisi, S. Batzner, Y. Xie, L. Sun, A. M. Kolpak, and B. Kozinsky, “On-the-fly active learning of interpretable Bayesian force fields for atomistic rare events,” *npj Comput. Mater.* **6**, 1–11 (2020).
- ¹⁴⁷N. Rønne, M. P. V. Christiansen, A. M. Slavensky, Z. Tang, F. Brix, M. E. Pedersen, M. K. Bisbo, and B. Hammer, “Atomistic structure search using local surrogate model,” *J. Chem. Phys.* **157**, 174115 (2022).
- ¹⁴⁸G. Csányi, T. Albaret, M. C. Payne, and A. De Vita, “Learn on the fly”: A hybrid classical and quantum-mechanical molecular dynamics simulation,” *Phys. Rev. Lett.* **93**, 175503 (2004).
- ¹⁴⁹Z. Li, J. R. Kermode, and A. D. Vita, “Molecular dynamics with on-the-fly machine learning of quantum-mechanical forces,” *Phys. Rev. Lett.* **114**, 96405 (2015).
- ¹⁵⁰R. Jinnouchi, F. Karsai, and G. Kresse, “On-the-fly machine learning force field generation: Application to melting points,” *Phys. Rev. B* **100**, 014105 (2019).
- ¹⁵¹C. J. Pickard, “Ephemeral data derived potentials for random structure search,” *Phys. Rev. B* **106**, 014102 (2022).
- ¹⁵²F. L. Thiemann, C. Schran, P. Rowe, E. A. Müller, and A. Michaelides, “Water Flow in Single-Wall Nanotubes: Oxygen Makes It Slip, Hydrogen Makes It Stick,” *ACS Nano* **16**, 10775–10782 (2022).
- ¹⁵³V. Kapil, C. Schran, A. Zen, J. Chen, C. J. Pickard, and A. Michaelides, “The first-principles phase diagram of monolayer nanoconfined water,” *Nature* **609**, 512–516 (2022).
- ¹⁵⁴M. Hellström, V. Quaranta, and J. Behler, “One-dimensional vs. two-dimensional proton transport processes at solid-liquid zinc-oxide-water interfaces,” *Chem. Sci.* **10**, 1232–1243 (2019).
- ¹⁵⁵M. Galib and D. T. Limmer, “Reactive uptake of N₂O₅ by atmospheric aerosol is dominated by interfacial processes,” *Science* **371**, 921–925 (2021).
- ¹⁵⁶T. A. Young, T. Johnston-Wood, V. L. Deringer, and F. Duarte, “A transferable active-learning strategy for reactive molecular force fields,” *Chem. Sci.* **12**, 10944–10955 (2021).
- ¹⁵⁷B. Monserrat, J. G. Brandenburg, E. A. Engel, and B. Cheng, “Liquid water contains the building blocks of diverse ice phases,” *Nat. Commun.* , 5757 (2020).
- ¹⁵⁸C. Schran, F. Briec, and D. Marx, “Transferability of machine learning potentials: Protonated water neural network potential applied to the protonated water hexamer,” *J. Chem. Phys.* **154**, 051101 (2021).
- ¹⁵⁹C. Zeni, A. Anelli, A. Glielmo, and K. Rossi, “Exploring the robust extrapolation of high-dimensional machine learning potentials,” *Phys. Rev. B* **105**, 165141 (2022).
- ¹⁶⁰C. Schran, F. Uhl, J. Behler, and D. Marx, “High-dimensional neural network potentials for solvation: The case of protonated water clusters in helium,” *J. Chem. Phys.* **148**, 102310 (2018).
- ¹⁶¹C. Schran, J. Behler, and D. Marx, “Automated Fitting of Neural Network Potentials at Coupled Cluster Accuracy: Protonated Water Clusters as Testing Ground,” *J. Chem. Theory Comput.* **16**, 88–99 (2020).
- ¹⁶²S. Chmiela, H. E. Sauceda, K. R. Müller, and A. Tkatchenko, “Towards exact molecular dynamics simulations with machine-learned force fields,” *Nat. Commun.* **9**, 3887 (2018).
- ¹⁶³J. S. Smith, B. T. Nebgen, R. Zubatyuk, N. Lubbers, C. Devereux, K. Barros, S. Tretiak, O. Isayev, and A. E. Roitberg, “Approaching coupled cluster accuracy with a general-purpose neural network potential through transfer learning,” *Nat. Commun.* **10**, 2903 (2019).
- ¹⁶⁴J. Daru, H. Forbert, J. Behler, and D. Marx, “Coupled Cluster Molecular Dynamics of Condensed Phase Systems Enabled by Machine Learning Potentials: Liquid Water Benchmark,” *Phys. Rev. Lett.* **129**, 226001 (2022).
- ¹⁶⁵M. S. Chen, J. Lee, H.-Z. Ye, T. C. Berkelbach, D. R. Reichman, and T. E. Markland, “Data-Efficient Machine Learning Potentials from Transfer Learning of Periodic Correlated Electronic Structure Methods: Liquid Water at AFQMC, CCSD, and CCSD(T) Accuracy,” *J. Chem. Theory Comput.* (2023), 10.1021/acs.jctc.2c01203.
- ¹⁶⁶B. Cheng, G. Mazzola, C. J. Pickard, and M. Ceriotti, “Evidence for supercritical behaviour of high-pressure liquid hydrogen,” *Nature* **585**, 217–220 (2020).
- ¹⁶⁷V. Zaverkin, D. Holzmüller, L. Bonferraro, and J. Kästner, “Transfer learning for chemically accurate interatomic neural network potentials,” *Phys. Chem. Chem. Phys.* **25**, 5383–5396 (2023).
- ¹⁶⁸Y. Litman, J. Behler, and M. Rossi, “Temperature dependence of the vibrational spectrum of porphycene: a qualitative failure of classical-nuclei molecular dynamics,” *Faraday Discuss.* **221**, 526–546 (2019).
- ¹⁶⁹D. M. Wilkins, A. Grisafi, Y. Yang, K. U. Lao, R. A. DiStasio, and M. Ceriotti, “Accurate molecular polarizabilities with coupled cluster theory and machine learning,” *Proc. Natl. Acad. Sci.* **116**, 3401–3406 (2019).
- ¹⁷⁰J. Westermayr, F. A. Faber, A. S. Christensen, O. A. V. Lilienfeld, and P. Marquetand, “Neural networks and kernel ridge regression for excited states dynamics of CH₂NH: From single-state to multi-state representations and multi-property machine learning models,” *Mach. Learn. Sci. Technol.* **1**, 25009 (2020).
- ¹⁷¹K. T. Schütt, M. Gastegger, A. Tkatchenko, K. R. Müller, and R. J. Maurer, “Unifying machine learning and quantum chemistry with a deep neural network for molecular wavefunctions,” *Nat. Commun.* **10**, 1–10 (2019).
- ¹⁷²A. Grisafi, A. Fabrizio, B. Meyer, D. M. Wilkins, C. Corminboeuf, and M. Ceriotti, “Transferable Machine-Learning Model of the Electron Density,” *ACS Cent. Sci.* **5**, 57–64 (2019).
- ¹⁷³S. J. Cox, “A theory for the stabilization of polar crystal surfaces by a liquid environment,” *J. Chem. Phys.* **157**, 94701 (2022).
- ¹⁷⁴V. Quaranta, J. Behler, and M. Hellström, “Structure and Dynamics of the Liquid-Water/Zinc-Oxide Interface from Machine Learning Potential Simulations,” *J. Phys. Chem. C* **123**, 1293–1304 (2019).
- ¹⁷⁵S. J. Cox, “Dielectric response with short-ranged electrostatics,” *Proc. Natl. Acad. Sci.* **117**, 19746–19752 (2020).
- ¹⁷⁶S. P. Niblett, M. Galib, and D. T. Limmer, “Learning intermolecular forces at liquid-vapor interfaces,” *J. Chem. Phys.* **155**, 164101 (2021).
- ¹⁷⁷A. Gao and R. C. Remsing, “Self-consistent determination of long-range electrostatics in neural network potentials,” *Nat.*

- Commun.* **13**, 1–11 (2022).
- ¹⁷⁸N. Artrith, “Machine learning for the modeling of interfaces in energy storage and conversion materials,” *J. Phys. Energy* **1**, 32002 (2019).
- ¹⁷⁹A. Singraber, T. Morawietz, J. Behler, and C. Dellago, “Parallel Multistream Training of High-Dimensional Neural Network Potentials,” *J. Chem. Theory Comput.* **15**, 3075–3092 (2019).
- ¹⁸⁰K. Schütt, P.-J. Kindermans, H. E. S. Felix, S. Chmiela, A. Tkatchenko, and K.-R. Müller, “SchNet: A continuous-filter convolutional neural network for modeling quantum interactions,” *Adv. Neural Inf. Process. Syst.* **30** (2017).
- ¹⁸¹J. Zeng, D. Zhang, D. Lu, P. Mo, Z. Li, Y. Chen, M. Rynik, L. Huang, Z. Li, S. Shi, Y. Wang, H. Ye, P. Tuo, J. Yang, Y. Ding, Y. Li, D. Tisi, Q. Zeng, H. Bao, Y. Xia, J. Huang, K. Muraoka, Y. Wang, J. Chang, F. Yuan, S. L. Bore, C. Cai, Y. Lin, B. Wang, J. Xu, J.-X. Zhu, C. Luo, Y. Zhang, R. E. A. Goodall, W. Liang, A. K. Singh, S. Yao, J. Zhang, R. Wentzcovitch, J. Han, J. Liu, W. Jia, D. M. York, W. E. R. Car, L. Zhang, and H. Wang, “DeePMD-kit v2: A software package for Deep Potential models,” *arXiv* (2023), 10.48550/arXiv.2304.09409.
- ¹⁸²N. Thomas, T. Smidt, S. Kearnes, L. Yang, L. Li, K. Kohlhoff, and P. Riley, “Tensor field networks: Rotation- and translation-equivariant neural networks for 3D point clouds,” *arXiv* (2018), 10.48550/arXiv.1802.08219.
- ¹⁸³M. Geiger and T. Smidt, “e3nn: Euclidean Neural Networks,” *arXiv* (2022), 10.48550/arXiv.2207.09453.
- ¹⁸⁴X. Gao, F. Ramezanghorbani, O. Isayev, J. S. Smith, and A. E. Roitberg, “TorchANI: A Free and Open Source PyTorch-Based Deep Learning Implementation of the ANI Neural Network Potentials,” *J. Chem. Inf. Model.* **60**, 3408–3415 (2020).
- ¹⁸⁵N. Artrith and A. Urban, “An implementation of artificial neural-network potentials for atomistic materials simulations: Performance for TiO₂,” *Comput. Mater. Sci.* **114**, 135–150 (2016).
- ¹⁸⁶R. Lot, F. Pellegrini, Y. Shaidu, and E. Küçükbenli, “PANNA: Properties from Artificial Neural Network Architectures,” *Comput. Phys. Commun.* **256**, 107402 (2020).
- ¹⁸⁷S. Chmiela, A. Tkatchenko, H. E. Sauceda, I. Poltavsky, K. T. Schütt, and K.-R. Müller, “Machine learning of accurate energy-conserving molecular force fields,” *Sci. Adv.* **3**, e1603015 (2017).
- ¹⁸⁸A. S. Christensen, L. A. Bratholm, F. A. Faber, and O. Anatole Von Lilienfeld, “FCHL revisited: Faster and more accurate quantum machine learning,” *J. Chem. Phys.* **152**, 44107 (2020).
- ¹⁸⁹M. K. Bisbo and B. Hammer, “Efficient Global Structure Optimization with a Machine-Learned Surrogate Model,” *Phys. Rev. Lett.* **124**, 086102 (2020).
- ¹⁹⁰A. Hajibabaei, C. W. Myung, and K. S. Kim, “Sparse Gaussian process potentials: Application to lithium diffusivity in superionic conducting solid electrolytes,” *Phys. Rev. B* **103**, 214102 (2021).

Supporting information for: Introduction to machine learning potentials for atomistic simulations

Fabian L. Thiemann,^{1,2} Niamh O'Neill,^{3,2,4} Venkat Kapil,^{3,4,5,6} Angelos Michaelides,^{3,4} and Christoph Schran^{2,4, a)}

¹⁾ *IBM Research Europe, Daresbury, Warrington, WA4 4AD, UK*

²⁾ *Cavendish Laboratory, Department of Physics, University of Cambridge, Cambridge, CB3 0HE, UK*

³⁾ *Yusuf Hamied Department of Chemistry, University of Cambridge, Lensfield Road, Cambridge, CB2 1EW, UK*

⁴⁾ *Lennard-Jones Centre, University of Cambridge, Trinity Ln, Cambridge, CB2 1TN, UK*

⁵⁾ *Department of Physics and Astronomy, University College London, London, UK*

⁶⁾ *Thomas Young Centre and London Centre for Nanotechnology, London, UK, London, UK*

(Dated: 2 October 2024)

OVERVIEW OF MACHINE LEARNING CONCEPTS

TABLE S1. Definition of important concepts.

Keyword	Definition
Machine learning	Draw inferences from patterns in data using algorithms
Supervised learning	Input data (structures) is provided by user and a desired output (energy, force) is learned by ML model.
ML model	Universal function with many parameters to be optimised
Regression	Transform structure to energy
Training set	Data used for optimisation
Test set	Data used to check transferability of model
Label	Reference energy (and forces) from electronic structure calculation
Hyperparameters	Parameters not optimised during learning task, but chosen by user (number of iterations in optimisation, size of model, ...)

^{a)} Electronic mail: cs2121@cam.ac.uk

OVERVIEW OF OPEN-SOURCE CODE

TABLE S2. Overview of different open-source codes to develop machine learning potentials.

Code	Description
HD-NNP	
RuNNer ¹³	Original implementation of HD-NNPs.
n2p2 ¹⁷⁹	Library based modular implementation of HD-NNPs with interface to Lammmps.
PhysNet ²¹	Tensorflow based message-passing NNP implementation built on physical principles for predicting energies, forces, dipole moments and partial charges.
SchNetPack ¹⁸⁰	Message-passing NN model based on pairwise distances with GPU accelerated MD code and output modules for dipole moment, polarizability, stress etc.
DeepMD ¹⁸¹	Deep NN model based on three body correlation functions with possibility of learning tensors.
MACE ^{20,90}	Interatomic potentials with higher order equivariant message passing and $\mathcal{O}(1)$ scaling with number of chemical species.
Nequip ²³	Based on tensor field networks ¹⁸² implemented in e3nn, ¹⁸³ a general framework for building E(3)-equivariant neural networks.
GPUMD ⁸⁷	GPU accelerated molecular dynamics code that supports neuroevolution potentials.
TorchANI ¹⁸⁴	PyTorch-based implementation of the ANI NNP.
aenet ¹⁸⁵	Training code for NNPs with interface to Tinker.
PANNA ¹⁸⁶	TensorFlow based package to train and validate NNPs with lammmps and ase interface.
Kernel-Based MLPs	
QUIP ¹⁴	Original implementation of the Gaussian Approximation Potential
pacemaker ^{17,86,88}	Tool for fitting of interatomic potentials in a general nonlinear Atomic Cluster Expansion form.
ACEsuit ⁸⁸	Various software packages surrounding the atomic cluster expansion written in Julia.
flare ¹⁴⁶	ACE descriptors coupled to sparse GP used for on-the-fly learning and interfaced to Lammmps.
sGDML ¹⁸⁷	Symmetric Gradient Domain Machine Learning implementation.
MTP ¹⁵	Original implementation of the Moment Tensor Potential.
FCHL ¹⁸⁸	MLP based on distribution functions of structural and alchemical parameters of atoms.
GOFFEE ¹⁸⁹	Efficient global structure optimization with a machine-learned surrogate model.
AutoForce ¹⁹⁰	Python package for sparse GPR of ab-initio PES.